DETERMINING THE OPTIMAL SPATIAL RESOLUTION TO ACCURATELY DISTINGUISH LAVA FLOW TYPES IN REMOTELY SENSED DATA: A STUDY OF LAVA FLOWS ON A SECTION OF MAUNA LOA'S NORTHEAST RIFT ZONE

A Senior Thesis

Presented To

The Faculty of the Department of Geology and Geophysics

School of Ocean and Earth Science and Technology

University of Hawai'i at Mānoa

In Partial Fulfillment

Of the Requirements for the Degree

Bachelor of Science

By

Donielle Mariko Chittenden

May 16, 2003

ACKNOWLEDGEMENTS

I would like to acknowledge NASA and the Hawai'i Space Grant Consortium for financially supporting my research. Assistance provided by these organizations enabled me to expand upon my undergraduate degree in Geology and Geophysics through the production of this thesis. Not only did the project allow me to gain experience in conducting research and analyzing data, but it also broadened my understanding of both planetary geology and volcanology. I thank my advisor, Scott Rowland, who was always so patient and took the time to explain basic behaviors and intricate details of volcanoes and lava flows. Thank you for your continued support and encouragement during this project.

Thanks also to Peter Mouginis-Mark for discussing lava flow characteristics and for providing me with ample amounts of helpful readings and research materials. Thanks to Jeffrey Taylor, who was always willing to "discuss fractals" and aided in the fractal analysis portion of the project.

Special thanks goes to one of my best friends, my boyfriend, Clint. All those late nights of studying and diligently editing my superfluous reports are finally paying off. Thank you for your dedication and patience with my never-ending study habits. I truly appreciate your constant support- as well as the numerous dinner deliveries to the POST building.

I want to especially thank my family, who has provided me with nothing but constant encouragement and unconditional love. Thanks to my sister, Brianne, and brother, Kyle, for being such wonderful companions and inspirations in my life. Thanks to my parents, Don and Cindi Chittenden, who have supported me in all my academic

and athletic endeavors, and whom I credit for making my entire college experience possible. Thank you, I love you all.

TABLE OF CONTENTS

LIST OF TABLES

LIST OF FIGURES

INTRODUCTION

Studying the physical properties of volcanoes, whether on Earth or on other planets, can provide insight about their past eruptive behaviors and help uncover the geological history of a specific area. By understanding the various forces and conditions required to create different volcanic features, confident speculations can be made on a volcano's origin and development. One surface feature that provides considerable information about volcanic processes is lava flows. Specific physical characteristics, such as lava flow thickness, width, and morphology, can help infer important eruption parameters, such as effusion rates and fountain heights. This type of information is valuable in gaining a heightened understanding of a volcano's development.

The two major identifiable types of basaltic lava flows are pāhoehoe and ʻaʻā (Rowland and Walker, 1990). Because they are produced by different eruptive styles, their distribution and frequency of occurrence can provide clues to the inner mechanics of a volcano. Each lava flow type is characterized by very distinctive surface properties, which are relatively simple to detect when observed in the field. When studying lava flows remotely, however, the classification process becomes more difficult due to the inability to easily detect these surface details.

The most accurate method of determining lava flow types is by conducting on-site fieldwork. In certain situations, however, this option is impractical and sometimes impossible. Traveling to different locations for extended amounts of time is financially straining to research budgets. The environmental conditions must also be considered because some are hazardous to humans. Both factors are not only hindering to the volcanic studies conducted on Earth, but are also impeding to planetary volcanic studies.

Thus, an alternative solution must be considered to overcome these obstacles.

Remote sensing is one technique for studying the physical surface properties of a volcano from a distance. It involves analyzing satellite images that display the amount of electromagnetic energy reflected off, or produced by, a surface. The main advantages of remote sensing are it provides a synoptic view of the focal area, it provides data on isolated or dangerous areas, and it allows researchers to study a feature through wavelengths beyond the visible range. Images of non-visible wavelengths may include thermal infrared or radar. Images of visible wavelengths display the features' "true colors", or colors detectable by the human eye. The images analyzed in this study covered the visible (0.4-0.7μm), near-infrared (0.7-3 μm), and mid-infrared (3-9μm) wavelengths of the electromagnetic spectrum.

There are four specific types of resolutions measured by remote sensing, namely spatial, temporal, radiometric, and spectral resolutions. This project focuses on the spatial resolution of an image provided by remotely sensed data. Spatial resolution, or the number of meters represented per image pixel, affects the ability to recognize certain features within an image. Features are usually more difficult to recognize if the pixels cover large dimensions. If the pixels represent smaller dimensions, however, then feature distinctions become more apparent.

A related technique that is helpful in examining lava flows through remotely sensed data is fractal geometry analysis. Fractals are shapes that are similar at all scales. If basaltic lava flows are fractal, then their margins should exhibit the same general shape at both close and distant proximities. A study by Bruno et al. (1994) tested this theory by measuring lava flow margins in the field and in satellite images. They concluded that

basaltic flows are indeed fractal, and that pāhoehoe and ʻaʻā flows have different fractal dimensions. Thus, determining lava flow type is possible in images of both high and low spatial resolutions by measuring its margins and calculating its fractal dimensions.

Satellite images provide detailed information on planetary surface features, but it is important to be aware of the limitations of imagery analysis. The focus of this research addresses the issue of preventing distorted interpretations of volcanoes when examined via satellite images. The methodology will include determining the criteria that characterize the two basaltic lava flow types in remote sensing images, and determining the optimal spatial resolution required for flow distinction through imagery analysis of a terrestrial volcano. The goal is to apply these results to distinguishing lava flow types on planetary volcanoes, thereby gaining a stronger understanding of their internal characteristics and eruptive patterns.

TERRESTRIAL ANALOGS

Scientists commonly refer to their geological understanding of the Earth as a basis for comparison of geologic features on other planets. The assumption is that features seen on other planets that resemble those found on Earth were probably formed by the same processes. Based on this assumption, it is practical to apply the knowledge of terrestrial volcanoes in explaining the developmental processes of similar volcanoes on other planets.

Several volcanoes located on other planets are categorized as shield volcanoes, which are broad structures with very gradual slopes (Chernicoff, 1999). Shield volcanoes result from the accumulation of successive basaltic flows that are able to spread to great

distances away from the vent. Most volcanoes observed on other planets dwarf those found on Earth (Wilson and Head, 1983). Reasons for this may include the fact that other planets lack plate tectonics, which can shift volcanoes away from the magma source, and often have lower surface gravities, which allow the volcanoes to rise higher and the lava flows to extend farther (Wilson and Head, 1994). Mauna Loa, for example, is the largest volcano on Earth, with a height of 10 kilometers and diameter of 120 kilometers. Olympus Mons, however, is the largest volcano on Mars and has a height of 25 kilometers, and a diameter of 624 kilometers (Mouginis-Mark et al., 1992).

Although Mauna Loa volcano is small compared to Olympus Mons, it is a shield

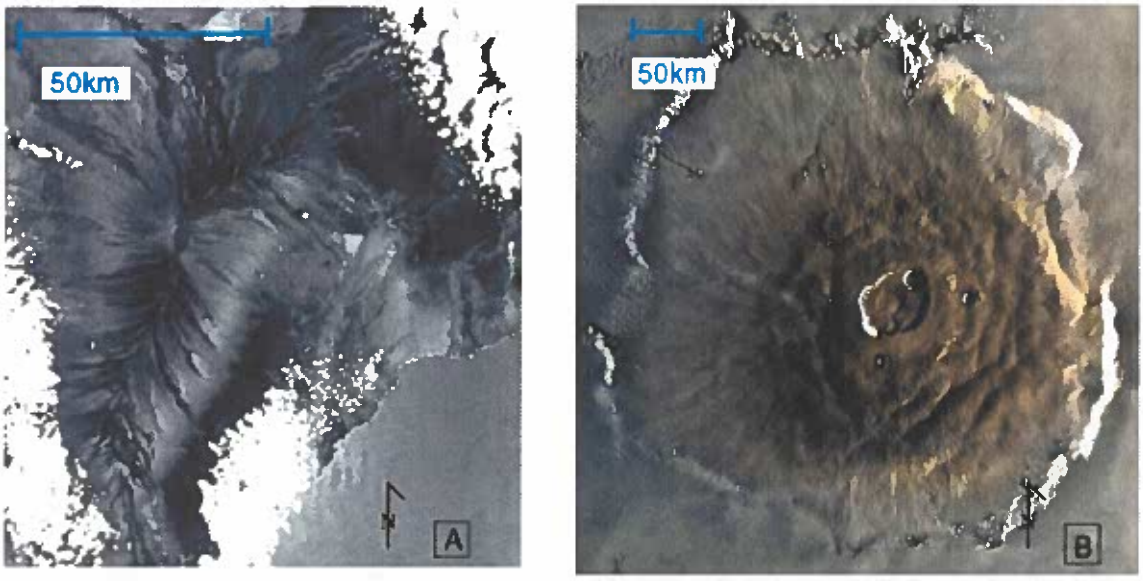

Figure 1- (A) MOC image of Mauna Loa, Hawai'i; 250m spatial resolution
(B) MOC image of Olympus Mons, Mars; spatial resolution unknown

volcano that is large by Earth standards and is often considered to be the closest terrestrial analogue to extraterrestrial shield volcanoes (Figure 1). Hence, research on Mauna Loa is encouraged to better understand the eruptive behavior and developmental processes of similar volcanoes on other planets. Due to its wealth of accessible

information, on-site researching convenience, and practicality to planetary studies, Mauna Loa was chosen for the terrestrial analog in this lava flow study.

BASALTIC LAVA FLOW TYPES

'A'ā and pāhoehoe lava flows are separated only by their differences in surface texture, not their chemical composition. The type of lava flow that forms from an eruption depends on the lava's cooling rate, velocity, and viscosity, or resistance to flow. In field observation, pāhoehoe lava flows have smooth, ropey surfaces that can form broad billows or lobes at the flow fronts (Macdonald, 1953). They are also characterized by a high percentage of spheroidal vesicles. Conversely, 'a'ā lava flows have rough, jagged surfaces with sharp, loose pieces of cooled lava that form on the top of the flow, known as clinkers (Figure 3). They have a low percentage of vesicles and the shapes of the vesicles are usually irregular (Macdonald, 1953).

Figure 2- Comparison between solidified pāhoehoe flows (left; Kilauea Volcano) and 'a'ā flows (right).

Pāhoehoe lava flows

Pāhoehoe flows are typical of lava that travel at slow speeds and have low viscosities, or move in a fluid-like manner (Macdonald, 1953). Due to their low mobility, these types of flows form flexible surfaces that stretch and fold, but do not separate or fail (Figure 3). Often, pāhoehoe flows also form lava tubes, which are enclosed within the flow. This occurs when the exposed surface of the flow cools, forming a tunnel within which lava can continue to travel (Peterson and Swanson, 1974; Peterson et al. 1994).

Lave tubes act as thermal insulators, allowing the lava inside the tube to continue flowing at a faster velocity than the surface layer. Oftentimes, even after the flow front has solidified, the interior lava remains molten and has the ability to rupture the outer skin of the original flow and continue traveling downslope. The formation that results is referred to as a pāhoehoe "toe", which will eventually solidify on the surface as well. Multiple toes form at pāhoehoe lava flow fronts either by several break-outs of lava from the central flow, or by rupturing the newly-formed toe and repeating the process (Macdonald, 1953). Lobe growth can continue as long as the rate of lava skin stretching exceeds the rate of skin thickening, a process enhanced by cooling (Rowland and Walker, 1990).

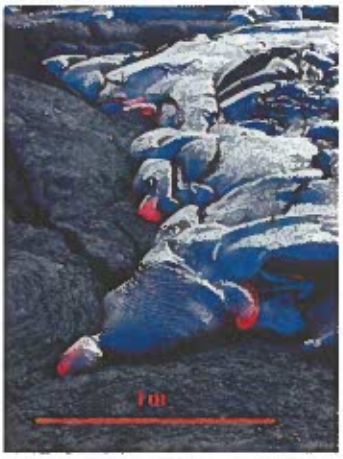

Figure 3- Pāhoehoe lava; Kilauea Volcano, November 2002

Once a lava tube solidifies and the lava completely drains out, its interior often remains hollow. With such a weak internal structure, it is common for the tops of the lava tubes to fracture and collapse. The openings caused by this structural failure are known as skylights (Figure 4) and are characteristic of pāhoehoe lava flows (Peterson and

Swanson, 1974). Lava tubes do not form from Hawaiian ʻaʻā lava flows.

Figure 4- Pāhoehoe skylight (left) formed by partial collapse of lava tube. Aerial view (right) of many skylights after flow solidification.

The low mobility rates of pāhoehoe flows allow the lava to retain its heat, inhibiting the degassing process of its volatiles. Thus, the gases are able to continue to expand even after flow movement has ceased. As the gas expands within the non-mobile substance, several well-rounded bubbles form, which result in spheroidal-shaped vesicles (Macdonald, 1953).

ʻAʻā lava flows

Figure 5- ʻAʻā lava flow; USGS website

ʻAʻā flows typically result from lava that is highly viscous, or resistant to movement, due to increased flow velocities. A heightened velocity, due to either an increase in downward slope of the topography or high effusion

rates, breaks the skin of the lava, exposing the hot interior to the cooler air. As the lava cools, its viscosity increases, and the tearing behavior on the surface layer is what causes the formation of the sharp, loose clinkers (Peterson and Tilling, 1979).

In contrast to the lava tubes formed by pāhoehoe flows, ʻaʻā lava flows usually form lava channels, which resemble river gullies and expose flowing lava to surface conditions (Rowland and Walker, 1990). As a lava flow travels downslope, its margins begin to cool at a faster rate than its interior. Because molten lava decreases in velocity as temperature decreases, the outer part of a viscous ʻaʻā flow will begin traveling at a much slower velocity than the lava traveling in the center of the flow. The buildup of lava and clinkers along the margins forms levees. Meanwhile, the middle part of the flow retains its high temperature and continues traveling downslope. This newly-formed channel provides a path for the lava, enabling it to travel quickly while retaining its heat. When the production of lava from the vent is exhausted, the remaining lava drains down the center of the flow. The result is a hollow channel of solidified basalt, with a smooth floor and rough, clinkery edges (Figure 6).

Figure 6- Solidified lava channel

Unlike pāhoehoe flows, ʻaʻā lava flows typically have low volatile contents. This may be in part due to high fountaining events, as well as a result of an increase in flow velocity. Because of their reduced amount of volatiles and enhanced cooling rates, the gases within ʻaʻā lava flows are able to stop expanding before the lava stops moving. As the lava continues downhill, the bubbles are stretched and twisted, resulting in irregularly-shaped vesicles (Macdonald, 1953).

Eruption Styles and their Associated Lava Flows

Whether a flow is pāhoehoe or ʻaʻā depends strongly on the eruption's effusion rate, or rate at which the lava flows out of the vent. ʻAʻā flows typically result from highly effusive eruptions that produce tall fountains, causing the lava to cool rapidly and break apart at the surface. Pāhoehoe flows are indicative of more placid eruptions that have low fountains and low effusion rates, which allow the lava to move at slower speeds and retain its smooth skin (Rowland and Walker, 1990). By characterizing the relative proportions of ʻaʻā to pāhoehoe on a particular volcano, geologists can infer its past eruptive behaviors.

REMOTE SENSING

Remote sensing involves making measurements or assessments of an object without having physical contact. Three main benefits of remote sensing include the abilities to study a large area at one time, to research an isolated or dangerous area, and to examine an area through electromagnetic wavelengths that are beyond the human visible range (e.g., thermal infra-red) (Jensen, 2000). The data are collected in the form of

digital images, which differ from photographs in that they are composed of pixels of equal dimensions. Each pixel has a numeric value that represents the intensity of an object's specific properties, such as color or temperature. Pixels of different values represent variations within images and display different colors to the human eye. These data can be displayed and manipulated by computer software for scientific studies.

Images of different spatial resolutions vary the size of the areas to be covered by each pixel. In images of low (i.e., coarse) spatial resolution, each pixel represents hundreds of meters of the ground surface. The ability to distinguish smaller objects is offset by these large parameters, but each image can cover vast areas. High (i.e., fine) spatial resolution images are composed of pixels with dimensions of approximately 1-20 meters of the ground surface. The result is a more detailed image that is able to display smaller objects within its view (Figure 7).

Although these detailed images are ideal for most remote sensing studies, there are some disadvantages in examining only images of high spatial resolutions. First, the feature characteristics provided by the "macro-view" are oftentimes sacrificed in the production of such detailed images; feature identification is simplified, yet transition areas and coverage factor are lost. Also, images of high spatial resolutions are not readily available for all areas because their data volumes are so large. Such data require more images to cover the same area, thus increasing the cost of complete area coverage. The optimal spatial resolution would be one that includes enough detail to accurately examine the image's features, but remains within the range of both the available data and research budget.

To accurately interpret remotely sensed data, enough detail must be included for

necessary distinctions of surface features. Usually, images of low spatial resolution are more accessible, but interpretations may be distorted due to the decreased amount of spatial detail provided. Images of high spatial resolution are more desirable because of the level of detail they are able to offer, but they are not always the most cost-effective for a particular project. By determining the coarsest spatial resolution that still allows for accurate study of specific features, such as lava flows, imagery interpretations can be considered reliable even without having access to images of high spatial resolutions.

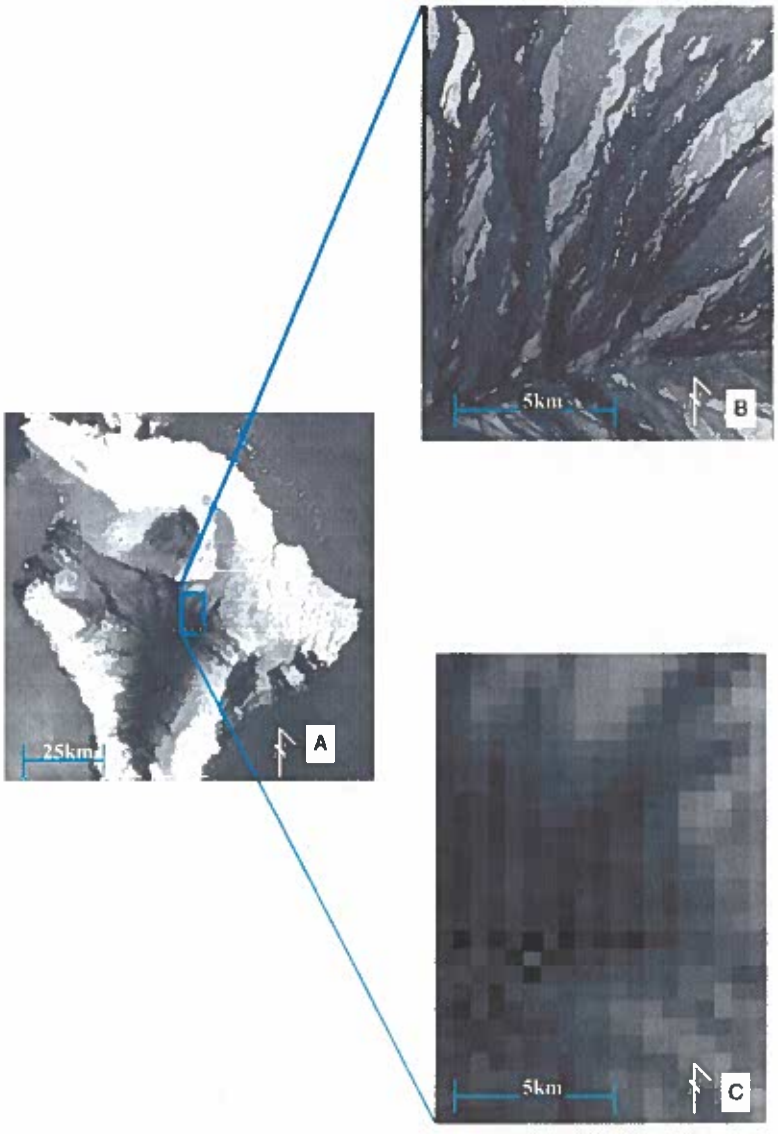

Figure 7- Comparing low and high spatial resolutions

(A) MODIS image of Mauna Loa on Big Island, Hawai'i, taken at 500m spatial resolution;
(B) IKONOS image of Mauna Loa taken at high (4m) spatial resolution.
(C) MODIS image taken at low (500m) spatial resolution. Depicts same area, and at the same scale, as image (B)

METHODOLOGY

This section of the paper describes the testing procedures and data analysis methods of the research project.

The steps involved in the research process were as follows:

- Determine a list of criteria to distinguish lava flow types in satellite images by examining aerial photographs of known flow types and researching their characteristics through previous studies
- Develop a quantitative method to systematically categorize lava flows as either ʻaʻā or pāhoehoe, based on the established criteria
- Assign flow types to lava flows on Mauna Loa's Northeast Rift Zone using satellite images with different spatial resolutions
- Confirm flow assignments with ground-truthing methods and mathematical models
- To conclude research, assess the data and compare the percentage of correct flow assignments from each image

Developing Distal-Flow Identification Criteria

Distinguishing lava flow types can be accomplished with relative ease while in the field. When viewing lava flows in remote sensing data, however, the decreased level of detail inhibits the ability to detect minute surface characteristics. In order to classify flow type through imagery analysis, the criteria to distinguish the flows must be modified to include the broader, macro-scale features. Although the "micro" qualities and properties are impossible to resolve individually in remote sensing data, they are still

considered important to the research study because they add to create a cumulative effect to the overall image.

By analyzing aerial photographs of a known-flow area, and acquiring supplementary information from Macdonald (1953), I was able to develop a list of criteria that served as a baseline in distinguishing flow types through satellite images. In black and white (panchromatic) images ʻaʻā generally has a lower albedo than pāhoehoe due to the shadowing effect that the ʻaʻā clinkers produce. This characteristic, however, depends on the relative age of the flow. Older flows may increase in albedo due to either the oxidization of iron (turning the flow color from black to red) or erosion of the jagged surface.

The smooth surfaces of pāhoehoe flows easily reflect the light, causing them to have higher albedos. ʻAʻā has more crenulated, cauliflower-shaped edges because its

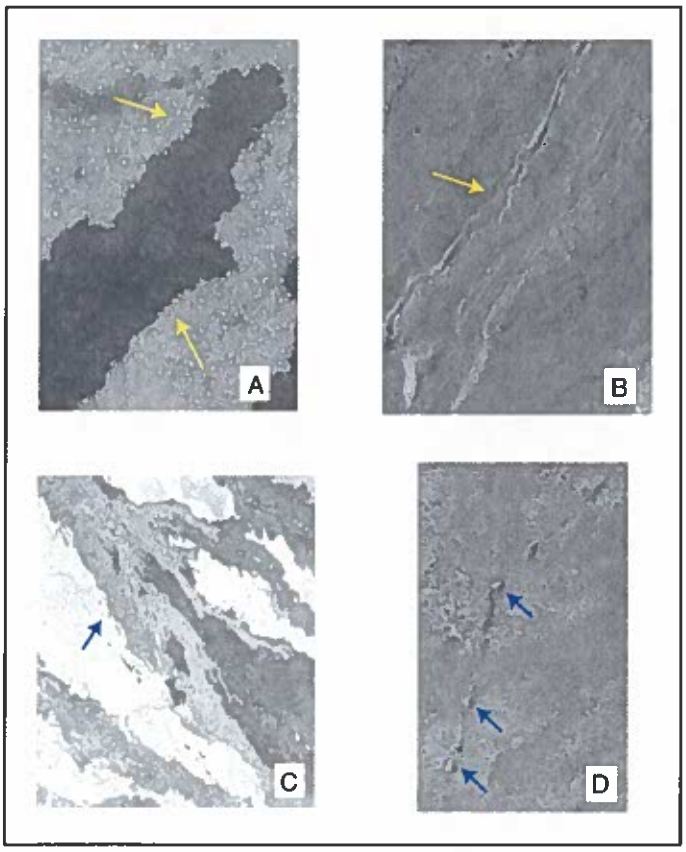

Figure 8- Lava flow characteristics (cropped from an IKONOS 4-m spatial resolution image)

(A)- ʻAʻā flow that has crenulated margins and low albedo; surrounded by vegetated pāhoehoe.

(B)- Lava channel shown in center of image, running from bottom left to upper right.

(C)- Flow of medium albedo in center is a pāhoehoe flow with convoluted edges situated atop ʻaʻā; lower albedo flow on left is also pāhoehoe.

(D)- Arrows indicate skylights found on pāhoehoe.

highly viscous nature does not allow for narrow branching arms to develop; pāhoehoe has sharper, more convoluted edges due to its ability to form smaller flow units. Other characteristics that aid in distinguishing the two flows include lava channels, which are indicative of ʻaʻā flows, or lines of skylights (that appear as small lineations), which indicate the collapse of a lava tube and hence a pāhoehoe flow (Figure 8). Tumuli, or larger slabs of lava broken apart due to inflation, are also characteristic features of pāhoehoe flows and may produce a mottled appearance in satellite images.

These are the criteria on which I based my lava flow assignments: flows of lower albedos, with crenulated edges, and/or lava channels indicate ʻaʻā; flows of higher albedos, with convoluted edges, and/or tumuli indicate pāhoehoe. The ability to distinguish such features is crucial for flow-type assignments. Because this ability varies with spatial dimension, it is important to determine the spatial resolution boundary beyond which such features become unnoticeable.

Quantifying the flow-type assignments

To quantify my assignments, I created a spreadsheet of the lava flows I outlined within each image. I also defined criteria that I could assign a numerical value to depending on whether it favored ʻaʻā or pāhoehoe. The criteria included: albedo (low or high), margin type (crenulated or convoluted), and the presence of certain diagnostic features (i.e. tumuli or lava channels). Depending on its distinct visibility, I assigned each feature a number between -3 and +3; a larger negative number indicated a more prominent ʻaʻā flow characteristic, and a larger positive number indicated a more prominent pāhoehoe flow characteristic. The overall sum of the flow features will be

referred to as a *flow number*. A flow with a negative *flow number* was identified as ʻaʻā, and a flow with a positive *flow number* was identified as pāhoehoe (see Table 2 for an example from the 30-m spatial resolution Landsat TM data).

A lava flow with a flow number close to zero indicated that it was difficult to categorize. Reasons for this include erosional effects, the presence of vegetation, or the occurrence of transition zones from pāhoehoe to ʻaʻā. Erosion of ʻaʻā flows would create smoother textures, resembling pāhoehoe flows from a distance. Likewise, vegetation that grows on pāhoehoe flows can create a darker appearance in satellite imagery. There is also the possibility for pāhoehoe flows to transition into ʻaʻā flows. If the velocity of a pāhoehoe flow increases, it might start to break apart and transition to an ʻaʻā flow. On the spreadsheet, I also marked which flows might possibly be transition zones. These intricate details were noted to account for any discrepancies found between my research and my fieldwork.

Satellite Imagery Analysis

Due to the vast number of satellite images available on the lava flows of Mauna Loa's Northeast Rift Zone, I decided to focus my research on this section of the volcano. The images I examined ranged in spatial resolution from 1000m to 4m (Table 1) and all were panchromatic images. The range included spatial resolutions that were obviously too low for accurate interpretations, but were necessary for bracketing the outer limit of the required range. The imagery analysis portion of my research began by first examining the satellite images of the lowest resolutions and continuing the process with images of higher spatial resolutions. Studying the images in this order enabled me to

assign flow types in images of low spatial resolutions without preconceived or biased insights.

The reason for examining panchromatic images is two-fold: radar and multi-banded images of some volcanoes are limited in number. Secondly, it is safe to assume that if these different lava flows are detectable at the crudest level of panchromatic images, they are most likely detectable in other image types as well. Radar images, for example, measure the radiowave and microwave wavelength energies emitted, or reflected, by an object (Jensen, 2000). Objects are sometimes easier to detect in these images because the wavelengths are able to highlight differences that are unnoticeable when examining only an object's visible wavelengths. Therefore, features distinguishable in panchromatic images are usually detectable in images of wavelengths beyond the visible range; however, not all features detected in the latter group of images are distinguishable in panchromatic images.

For this project, I analyzed a total of 19 satellite images. In some cases, more than one wavelength was available at a particular spatial resolution. Table 1 describes the type of images examined along with their respective spatial resolutions and wavelengths. In Adobe Illustrator, I traced the outlines of identifiable flow margins (Figure 9) and labeled each flow as ʻaʻā, old ʻaʻā, or pāhoehoe, based on its flow number; old ʻaʻā contains the same characteristics as ʻaʻā flows, but is not as low in albedo. The purpose for indicating old ʻaʻā was to justify categorizing a flow of high albedo as ʻaʻā. Because both old and young pāhoehoe flows have high albedos, distinction between the two was not necessary.

Starting with one of the low spatial resolution images, I assigned each detectable flow an identification number (Figure 9; Table 2). The flow retained this number through every image, and consecutive numbers were assigned to "new" flows that became apparent in the higher spatial resolution images. This method helped me to track the same flow within separate images, and to test whether I would categorize it differently from one image to the next. Figure 10 shows a 250-m spatial resolution image for a comparison to the high spatial resolution image. Only the letters A ('a'ā), P (pāhoehoe), and OA (old 'a'ā) appear on the image because individual flows are not detectable at this spatial resolution.

Table 1- List of all images examined. Includes names of satellites that provided image (Image Type), spatial resolutions (m), and wavelengths (μm)

Image Type	**Spatial Resolution (m)**	**Wavelength (μm)**
IKONOS	4	Near-IR (0.75-0.90)
IKONOS	4	Red visible (0.63-0.69)
SPOT	10	All visible (0.52-0.9)
Landsat	15	All visible (0.52-0.9)
SPOT	20	Near-IR (0.75-0.90)
SPOT	20	Red visible (0.63-0.69)
Landsat	30	Blue visible (0.45-0.52)
Landsat	30	Near-IR (0.75-0.90)
Landsat	30	Mid-IR (1.55-1.75)
MSS	60	Blue visible (0.45-0.53)
MSS	60	Green visible (0.52-0.60)
MSS	60	Red visible (0.63-0.69)
MSS	60	Near-IR (0.76-0.90)
MODIS	250	Red visible (0.62-0.67)
MODIS	250	Near-IR (0.84-0.88)
MODIS	500	Blue visible (0.46-0.48)
MODIS	500	Mid-IR (1.23-1.25)
MODIS	1000	Blue visible (0.44-0.45)
MODIS	1000	Near-IR (0.86-0.88)

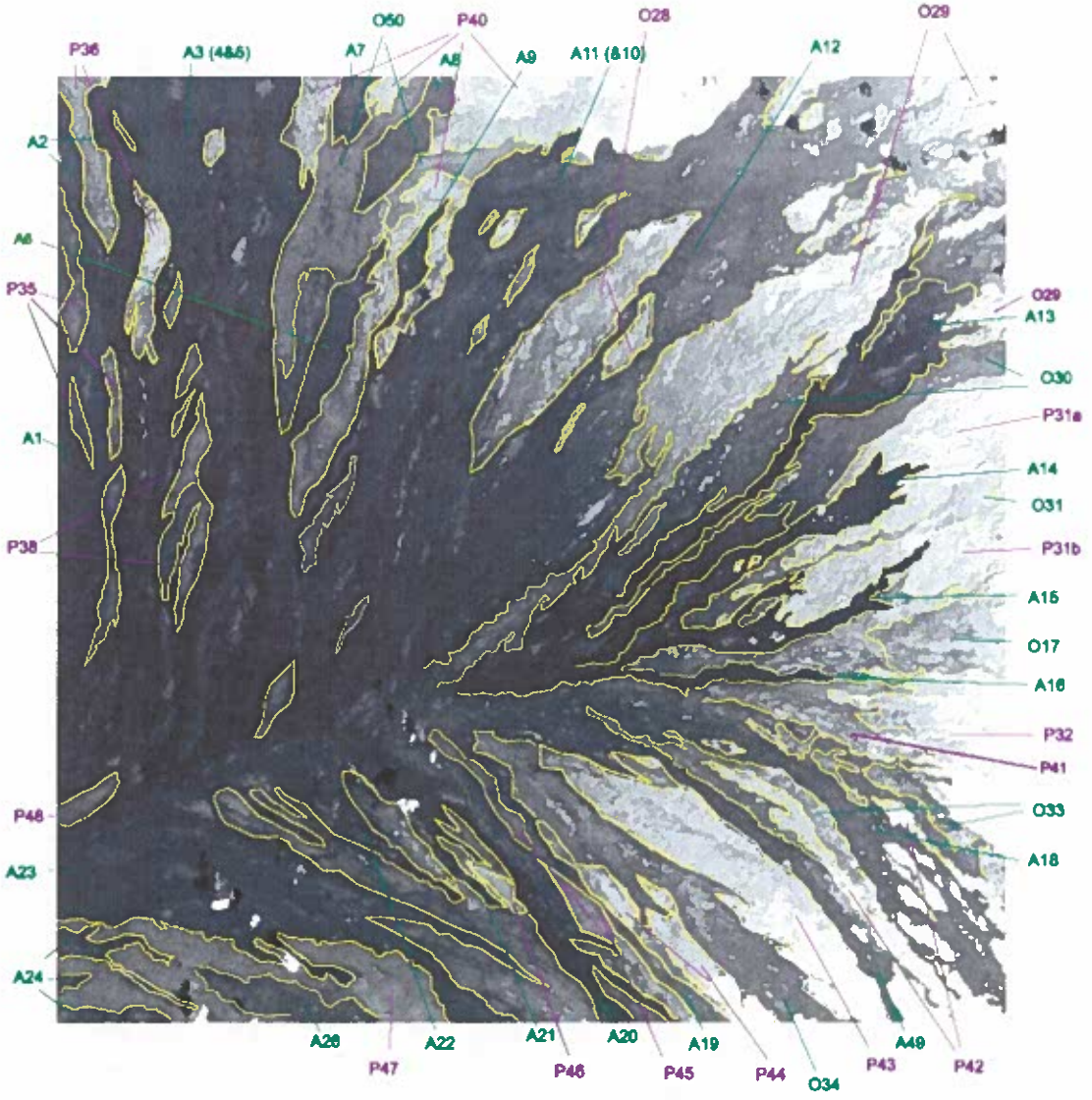

Figure 9- Example of flow outlines created in Adobe Illustrator; number represents flow identification number; purple lines indicate flows assigned as "Pāhoehoe"; green lines indicate flows assigned as "'A'ā". The letters "P" and "A" were added to the flow ID numbers after the categorization process for easy reference while working in the field.

Table 2- Quantifying the flow assignment process
ID# Refers to flow outlined in Figure 9
The flow number is found under the "Total" column; negative numbers represent 'a'ā flows and positive numbers represent pāhoehoe flows. The "Actual Flow Type" column indicates the flow type determined by the fieldwork.
--- Symbols indicate the lava flow was not detected in this particular image

Image: Landsat_04; 30m spatial resolution; near IR wavelength

ID#	Low Albedo	Crenulated Edges	Internal Flow Lobes	High Albedo	Convoluted Edges	Tumuli Present	Transition Zone	Total	Assigned Flow Type	Actual Flow Type
1	-3	-2	0	0	1	0	0	-4	A	
2	-3	-3	0	0	0	0	0	-6	A	
3	-3	-2	0	0	0	0	0	-5	A	A
4	see 3									
5	see 3									
6	-3	-2	0	0	1	0	0	-4	A	A
7	-3	-2	0	0	1	0	0	-4	A	A
8	-3	-3	0	0	0	0	0	-6	A	A
9	-3	-2	0	0	1	0	0	-4	A	A
10	-3	-3	-2	0	0	0	0	-8	A	A
11	see 10									
12	-2	-2	-1	0	1	0	0	-4	A	P
13	-3	-1	0	0	2	0	0	-2	A	A
14	-3	-1	0	0	2	0	0	-2	A	A
15	-3	-2	0	0	1	0	0	-4	A	
16	-3	-2	0	0	2	0	0	-3	A	
17	-2	-1	-2	2	2	1	X			
18	-3	-2	-1	0	2	0	0	-4	A	
19	-2	0	-1	1	2	0	X			
20	-3	-2	0	0	2	0	0	-3	A	
21	-3	-2	0	0	2	0	0	-3	A	
22	-3	-2	0	0	2	0	0	-3	A	
23	-3	-2	-2	0	2	0	0	-5	A	
24	-3	-2	0	0	2	0	0	-3	A	
25	see 24									
26	-3	-2	0	0	-1	0	0	-6	A	
27	see 3									
28	-2	0	-3	2	2	0	0	-1	A	P
29	-2	0	-3	2	2	0	0	-1	A	A
30	-3	-1	-1	0	1	0	0	-4	A	A
31	-2	-1	-2	2	2	0	0	-1	A	A
31a	0	0	0	3	3	0	0	6	P	P
31b	0	0	0	3	3	0	0	6	P	P
32	-1	0	-1	1	3	1	X	3	P	
33	-2	-2	0	0	0		X	-4	A	
34	-3	-1	-2	0	1	1	0	-4	A	
35	0	0	0	3	0	1	0	4	P	
36	0	0	0	3	0	1	0	4	P	
37	-	-	-	-	-	-	-			
38	0	0	0	2	0	1	0	3	P	
39	-	-	-	-	-	-	-			
40	0	0	0	3	1	1	0	5	P	
41	-1	0	0	2	3	1	X	5	P	
42	0	0	0	3	1	2	0	6	P	
43	0	0	0	3	1	1	0	5	P	
44	0	0	0	3	2	2	0	7	P	
45	-1	0	0	2	1	2	0	4	P	
46	0	0	0	3	0	1	0	4	P	
47	0	0	0	3	2	1	0	6	P	
48	-1	0	0	2	0	1		2	P	
49	-3	-3	0	0	0	0	0	-6	A	
50	-2	-2	-2	1	0	0	0	-5	A	A

Number values:
(-3) : dominant 'a'a feature
(-2) : 'a'a feature occurs throughout most of flow
(-1) : 'a'a feature detected in parts of flow
(0) : feature undetectable
(1) : pahoehoe feature detected in parts of flow
(2) : pahoehoe feature occurs throughout most of flow
(3) : pahoehoe feature dominant

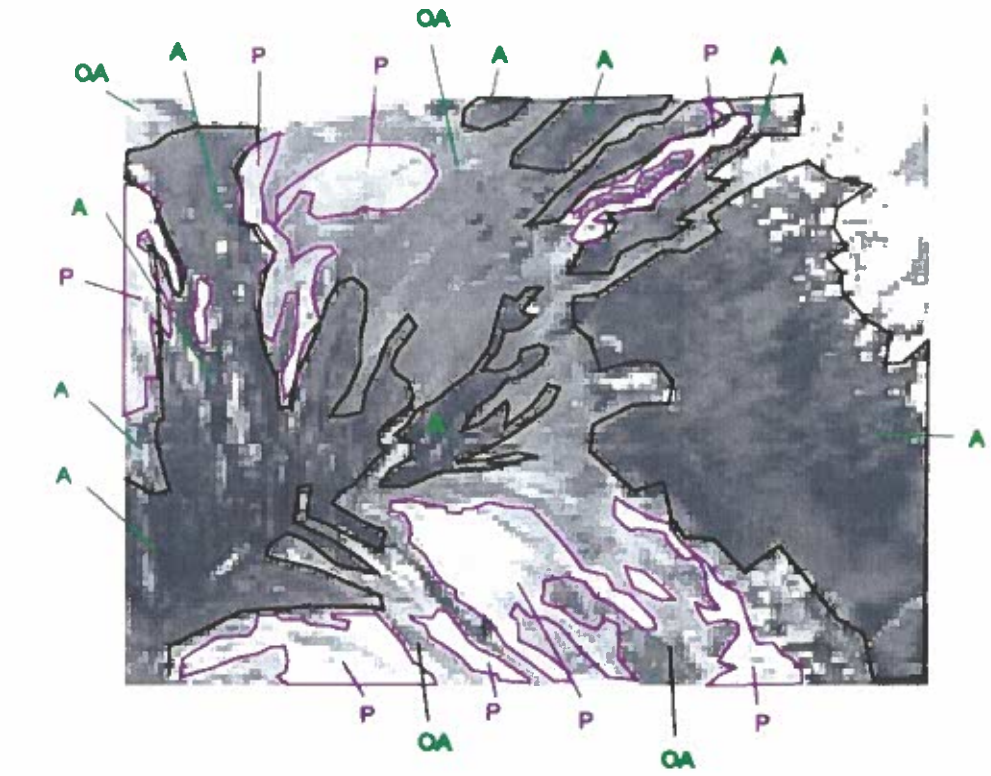

Figure 10- Image of the same area covered in Figure 9, but at 250 m spatial resolution. 'A' represents 'a'ā, 'P' represents pāhoehoe, and 'OA' represents old 'a'ā. Notice the assigned areas do not have numbers because they were not considered individual flows. Entire areas were assigned as pāhoehoe or 'a'ā, but numbers were not designated at this spatial resolution; thus, no table is available to show a quantitative analysis as in Table 1.

Fieldwork

In order to confirm or refute the flow assignments made from the satellite images, I traveled to Mauna Loa to obtain ground-truthing data. By walking across the lava flows and tracking my positions with a GPS, I was able to locate specific flow margins and lava flow types in the field. Differentiating lava types was eased by the ability to see smaller details in the lava's surface texture, and I was able to record the actual flow types of 16 flows in the mapping area. Because field time was limited, I focused primarily on the areas in which the flow types were difficult to distinguish in satellite imagery. These

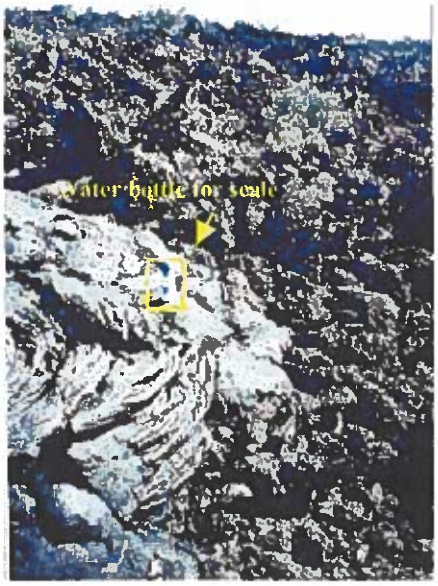

Figure 11- Photo taken while working in the field; shows clear margin between two lava flows. Pāhoehoe flow (left) overlying surrounding ʻaʻā flow.

particular lava flows had flow numbers that were close to zero in the quantitative spreadsheet, and thus contained the highest possibility for error in flow-type assignment. Another purpose for concentrating on them was to target the specific causes for any incorrect assignments so that such errors in future flow-determination studies could be avoided.

During the fieldwork analysis, I did find a few flows that had been categorized incorrectly. Within close proximity to the flows, the reasons for the errors were apparent: erosion, vegetation, and transitional zones all aided in distorting the identification process (Figure 12). For instance, even in images of the finest spatial resolutions, I had assigned flow #12 as "old ʻaʻā" due to its low albedo, and semi-crenulated edges (Figure 9, flow #A12). Upon field observation, however, this flow was actually old, weathered, and vegetated pāhoehoe. Another flow that appeared to be an entire area of pāhoehoe turned out to have patches of ʻaʻā flow textures, indicating that it may have been a transition zone (Figure 9, flow #P40).

Figure 12- Photo taken while working in field; shows clear distinction between two different flows, but both are ʻaʻā. The light brown flow (right) is much older than the darker flow on the left. The change in color is due to weathering processes. In satellite images, the flow on the right may be confused with a pāhoehoe flow due to its higher albedo.

RESULTS

Assigning flow numbers, combined with field checking, allowed for semi-quantitative analysis of flow identification. Two important factors vary significantly with respect to spatial resolution: total number of identifiable flows, and the correct assignment of flow type. Both the number of identifiable flows and the percentage of correct flow assignments decreased with coarsening spatial resolution. Many flows, seen in images of higher spatial resolutions, were not even detectable in the images of 500-m and 1000-m spatial resolutions. Figure 13 plots the total number of flows per square kilometer versus spatial resolution. It shows that the ratio drastically decreases beyond 30 m spatial resolution, implying the ability to accurately interpret flow types reduces beyond this spatial resolution.

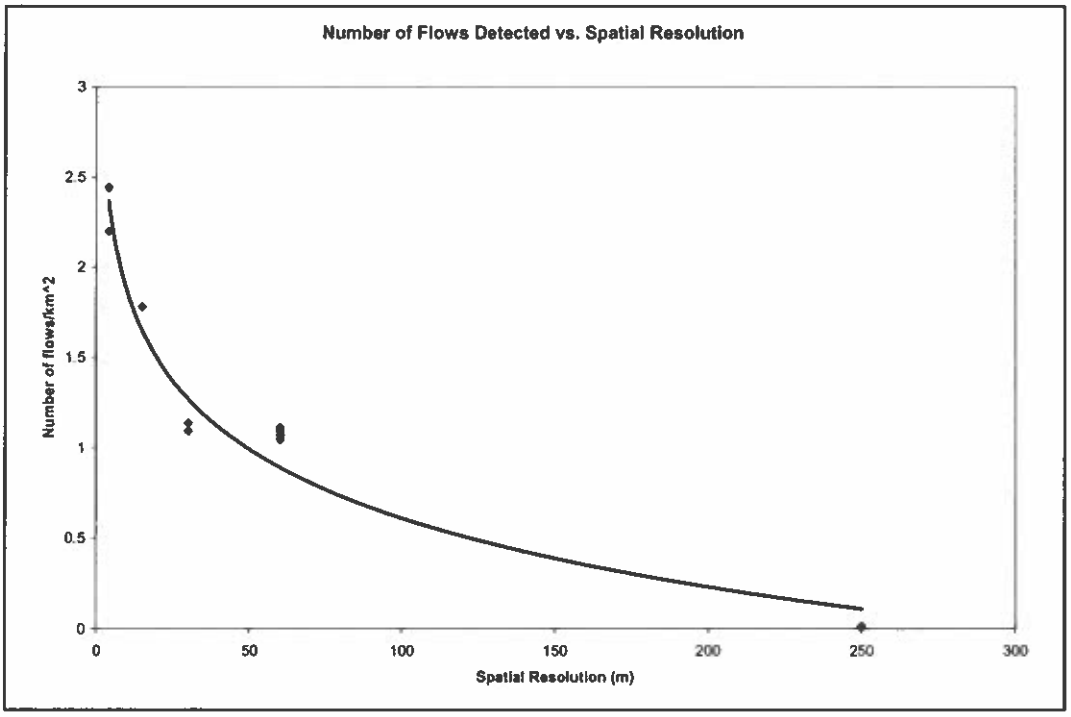

Figure 13- Graph comparing the number of total flows per square kilometer that were detected at each spatial resolution interval.

Due to the limited amount of field time, I was only able to check 16 flows in the field, out of the 50 flows examined in the high spatial resolution images. When I compared my field observations to the flow assignments at the 4-m and 10-m spatial resolution images, 11 out of 16 (70%) of the assignments were correct. This percentage remained constant for the images of 15 m, 20 m, and 30 m spatial resolutions. When comparing the observations to the flow assignments of the 60-m spatial resolution images, however, only 9 out of 16 (55%) were correct (Figure 14).

The low percentages are due to the small number of total flows I was able to confirm. Also, seven of these 16 flows had flow numbers that were close to zero (from the quantitative analysis), indicating that they were difficult to categorize in imagery analysis. These flows were specifically targeted to understand the causes of flow assignment errors, but they also decreased the percentages of correct flow-type assignments.

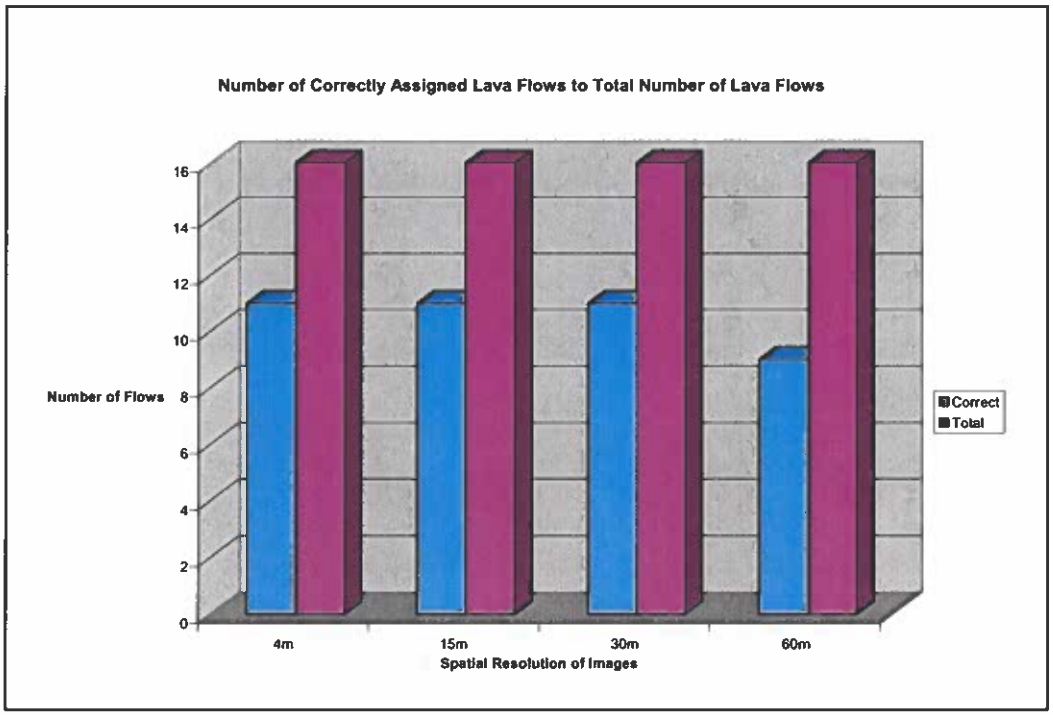

Figure 14- Graph comparing the number of correct flow assignments to total number of flows for each spatial resolution interval

The examination of constant resolution images at different wavelengths proved to be an important aspect to the study. Some margins became more prominent when comparing images of an area at the same spatial resolution, but at different wavelengths. For example, one margin between vegetated pāhoehoe and ʻaʻā was much more visible in the mid-IR (mid-infrared, 1.55-1.75μm) image than in the blue visible (0.45-0.52μm) image. (Figure 15). Therefore, it would be ideal to analyze several images of the same area at different wavelengths, or even multi-banded images, before determining the margins and assigning the flow types.

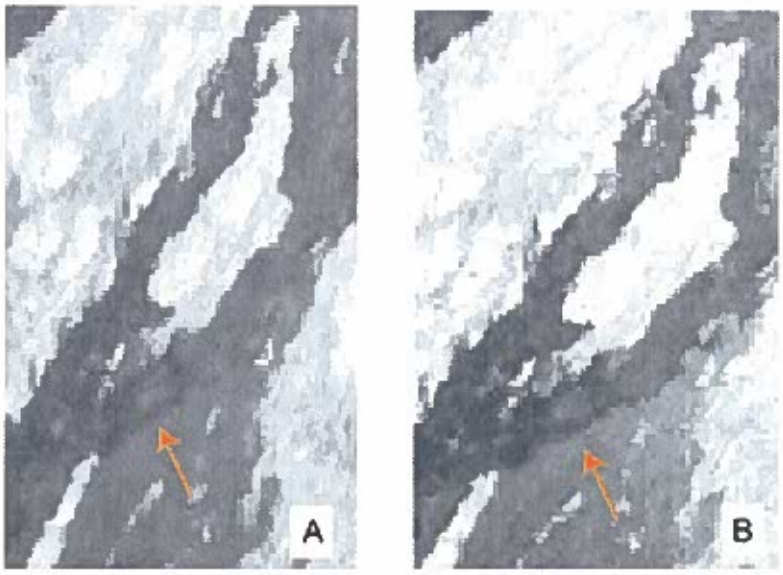

Figure 15- Arrows point to a lava flow margin, which is easier to detect in (B) than in (A). Both images are Landsat TM images of 30 m spatial resolution, but (A) displays the near-IR wavelengths whereas (B) displays the mid-IR wavelengths.

FRACTAL ANALYSIS

Within the imagery analysis portion of this project, I was able to study and assign flow types of up to 50 flows in the images of highest spatial resolutions along Mauna Loa's Northeast Rift Zone. However, due to time and budget constraints, I was only able to confirm 16 flows while in the field. This may seem to be a low ratio on which to base

my research, but oftentimes volcanic research cannot be complimented by any fieldwork. For example, a volcano may be situated either in a remote area, where access is highly limited, or on another planet, where access is completely denied. In these instances, a second remote method of analysis would be helpful to support geological interpretations made from satellite image observations. For this project, I decided to conduct a small test to determine if fractal analysis of these flows could augment (or substitute, if necessary) field observations.

Fractals are features that have a characteristic shape regardless of the scale. These individual features combine to form an object that exhibits the same overall shape (Turcotte, 1992). As concluded in the study by Bruno et al. (1994), basaltic lavas are fractal. Thus, basaltic lava flow margins should exhibit self-similar features that are scale invariant.

An object's "fractal dimension" can be calculated by following a series of mathematical formulas that basically measure an object's level of convolution. Convoluted objects have high fractal dimensions, whereas smooth objects have low fractal dimensions (Turcotte, 1992). Bruno et al. (1994) showed that pāhoehoe flows have higher fractal dimensions than ʻaʻā flows. This is due to the convoluted pattern of pāhoehoe flows in comparison to ʻaʻā flows. The study concluded that pāhoehoe flows usually have fractal dimensions of 1.15 or greater. ʻAʻā flows commonly have fractal dimensions of 1.09 or smaller.

For this project, I measured the fractal geometry of the lava flow margins aided by the computer program, Benoit Fractal Analysis System. The Benoit computer program is able to determine the fractal dimension value by measuring the degree of

convolution of a line in an image. The calculated fractal dimension helped to categorize a lava flow as either ʻaʻā or pāhoehoe.

To determine whether the computer program would be applicable to this study, I tested the margins of known flow types at different spatial resolutions to check for consistent results. First, I focused on two known lava flows from Mauna Loa- one being pāhoehoe, the other being ʻaʻā- from images between 4 m and 60 m spatial resolutions. The test was limited to this spatial resolution range because the margins of the flows were undistinguishable in the images of spatial resolutions coarser than 60 meters. Next, I created digital outlines of a section of each flows' margin in Adobe Illustrator. By inserting the outlines into the program, I was able to obtain their fractal dimensions.

Figure 16 shows the results of the Benoit computer test. The graph compares the fractal dimensions of both the pāhoehoe and ʻaʻā flows at different spatial resolutions. It shows that the fractal dimensions for both flow types fall within the ranges determined by Bruno et al. (1994). Based on these results, I consider the Benoit computer program to be sufficient for accurate basaltic flow-type categorization within the 4 m to 60 m spatial resolution range.

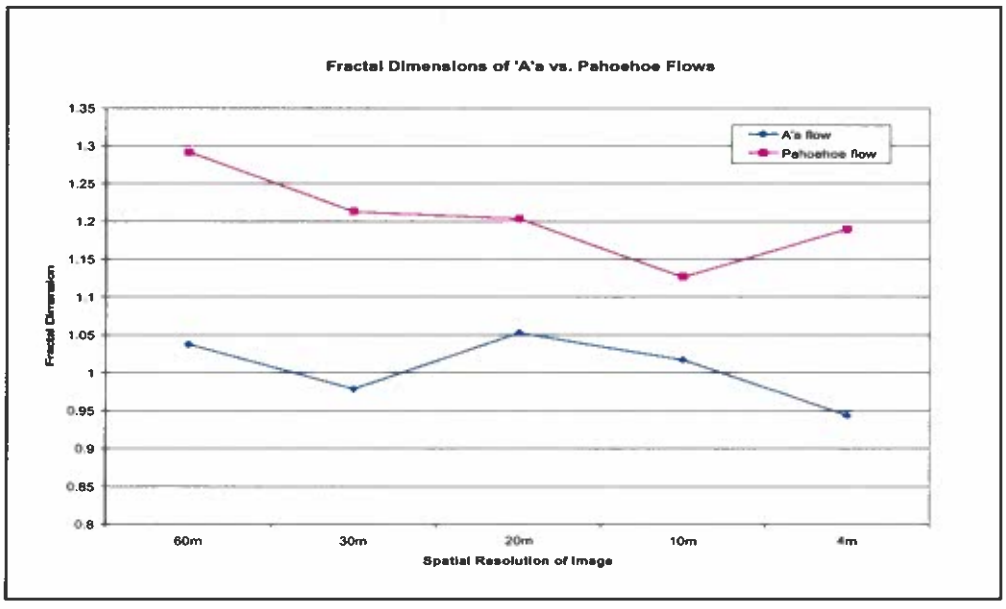

Figure 16- Results of the Benoit computer program. The fractal dimension range for ʻaʻā flows was 0.94-1.05; optimal range is 1.09 or lower. Pāhoehoe flows ranged in fractal dimensions from 1.13-1.29; optimal range is 1.15 or higher.

FUTURE STUDIES

One drawback to fractal analysis of lava flows is that it relies on measuring the *margins* of the lava flows to determine the flow type. If, however, the margins of the flow in question are covered by another lava flow, the method cannot be applied. For this reason, lava flow studies cannot completely rely upon fractal geometry to distinguish the flow type. Thus, the study of surface characteristics remains a crucial aspect to flow-type determination.

Possible future studies for this project include expanding upon the types of images analyzed to include radar or thermal infrared wavelengths; determining the spatial resolution limit of accurate lava flow interpretations through fractal analysis; or applying the methods used in this study to accurately map lava flows on another planet.

It is also important to compare images of similar spatial resolutions, but at different wavelengths. Occasionally, features detected at one wavelength are indistinguishable at another. As shown in Figure 15, one of the flow margins is easier to detect in the Landsat TM mid-IR wavelength versus the Landsat TM near-IR wavelength.

As for fractal analysis, the theory is based on the premise that fractals are scale-invariant, but there must be a specific spatial resolution limit for this method as well. Although there are certainly different causes of the meso-scale variations on a flow versus the macro-scale variations, a limit will exist because the ability to detect margins in low spatial resolution images eventually becomes impossible. If the margins are very difficult to detect in an image, it will not be possible to create outlines for fractal measurements.

CONCLUSIONS

After analyzing numerous satellite images at a range of spatial resolutions and completing fieldwork to support my research, I found that the coarsest spatial resolution required to accurately interpret lava flow type is 30 meters. Images of 1000 m and 500 m spatial resolutions did not include enough detail to see the individual lava flows (Figure 7). The images of 250 m spatial resolution could detect differences in albedo, a key differentiating factor between ʻaʻā and pāhoehoe, but the individual flow outlines were still a challenge to distinguish. In the 60 m spatial resolution images, individual lava flows finally came into view; however, not all the flow margins were clearly apparent until I examined the images of 30 m spatial resolution (Figure 13).

Lava flow characteristics became much more distinguishable in the images with spatial resolutions that were finer than 30 meters. Details, such as lava channels, vegetation, and convoluted versus crenulated margins became more and more visible, simplifying the categorization process. Because the flow-type assignments in the 30 m spatial resolution data were consistent with the flow types determined in the images of finer spatial resolutions, the conclusion is that lava flow interpretations within this range are valid and reliable. High spatial resolution images are the most desirable for discerning minute lava flow details, but images that include broad areas and enough detail for flow-type categorization are the most desirable for examining a multiple of flows at one time.

By understanding the detail of satellite imagery, and its effective use at various resolutions, the accuracy of feature identification and interpretation will increase when studying areas through remote sensing. Despite the lack of available physical samples,

remote sensing has become a dependable method from which to obtain valuable information on surface features. Studies of volcanoes located on Earth, or on other planets, are no longer impeded by restricted access to isolated areas. Applying this knowledge to other volcanological studies will broaden the general understanding of volcanic developmental processes, thereby gaining an even larger background regarding the geological history of the Earth.

APPENDIX A

Satellite Images

Attached are the satellite images examined in this project. The figure below is a 500-m spatial resolution image of the Big Island, Hawai'i. The box indicates the research location (part of Mauna Loa's Northeast Rift Zone), and the subsequent images display only that particular section of the volcano. 'A' is 'a'ā; 'P' is pāhoehoe; 'OA' is old 'a'ā.

*Note: Due to computer disk failures during the research, some images are missing from the appendix

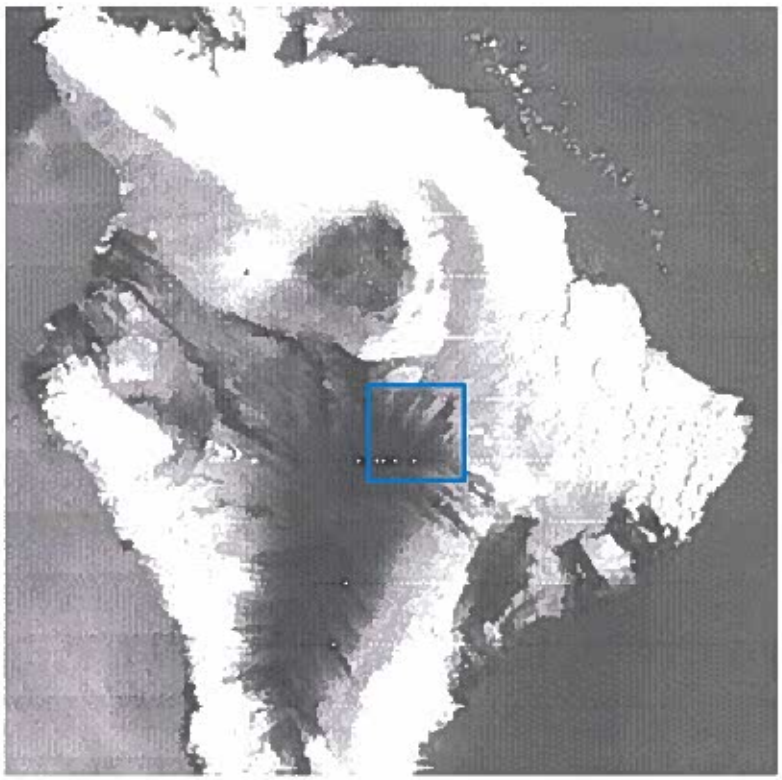

Figure A1- MODIS image at 500 m spatial resolution; mid-IR wavelengths (1.23-1.25 μm)

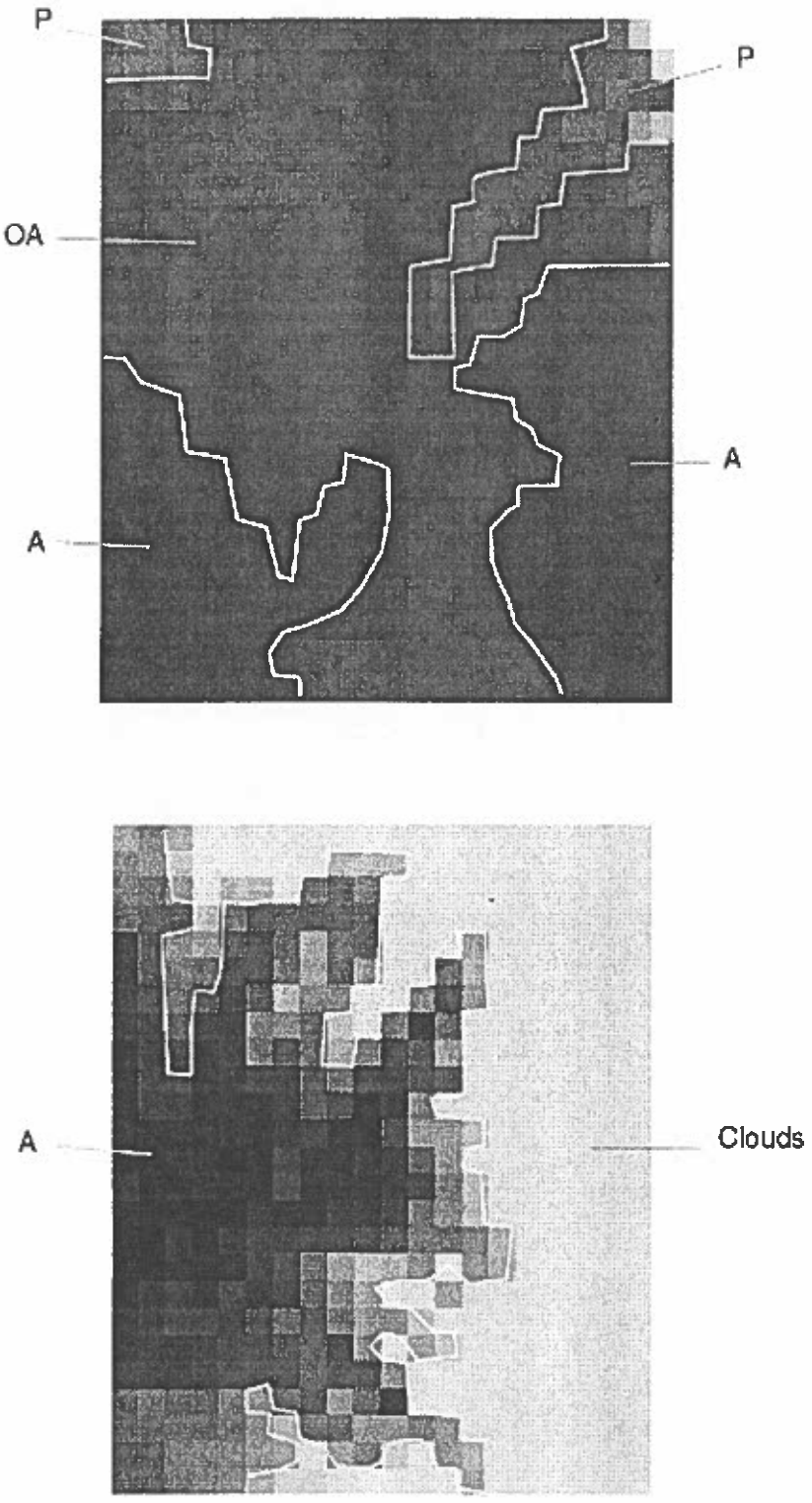

Figure A2- (Top)- MODIS image at 1000 m spatial resolution; blue visible (0.44-0.45 μm);
(Bottom)- MODIS image at 1000 m spatial resolution; near-IR (0.86-0.88 μm);
Individual flows are not detectable in either image; letters correspond to areas, not specific flows

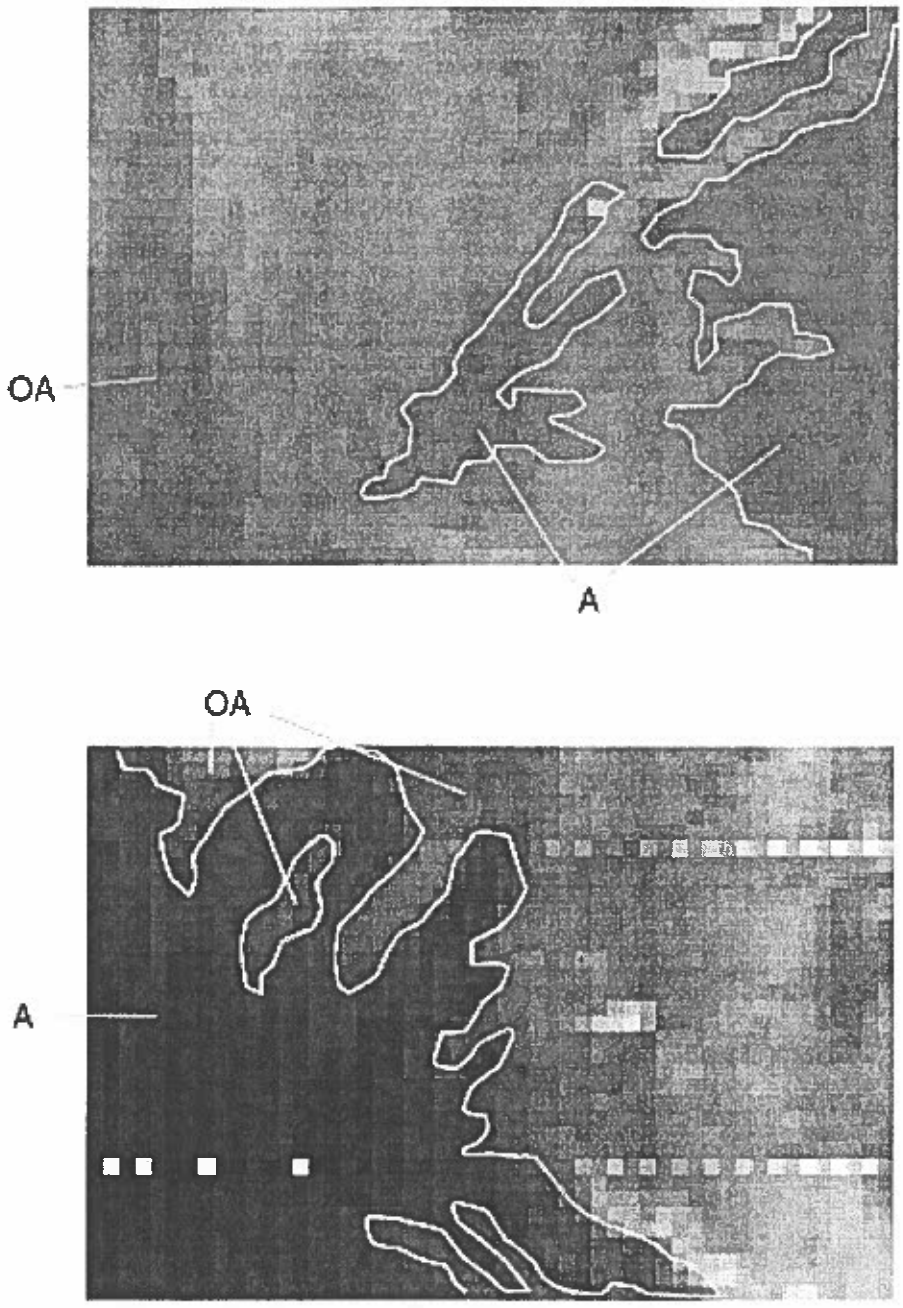

Figure A3- (Top)- MODIS image at 500 m spatial resolution; blue visible (0.46-0.48 μm);
(Bottom)- MODIS image at 500 m spatial resolution; mid-IR (1.23-1.25 μm);
Individual flows not apparent in either image; letters correspond to entire areas, not specific flows

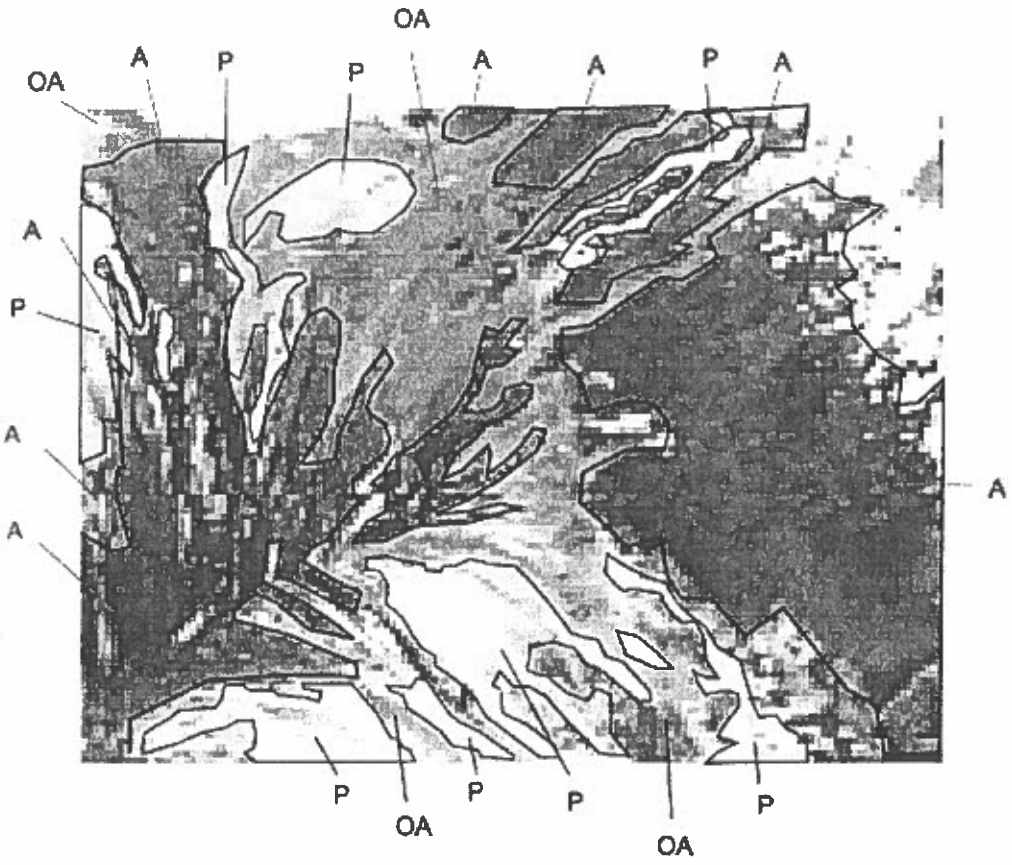

Figure A4- MODIS image at 250 m spatial resolution; red visible (0.62-0.67 μm); flows are becoming more apparent, but individual flows are still undetectable.

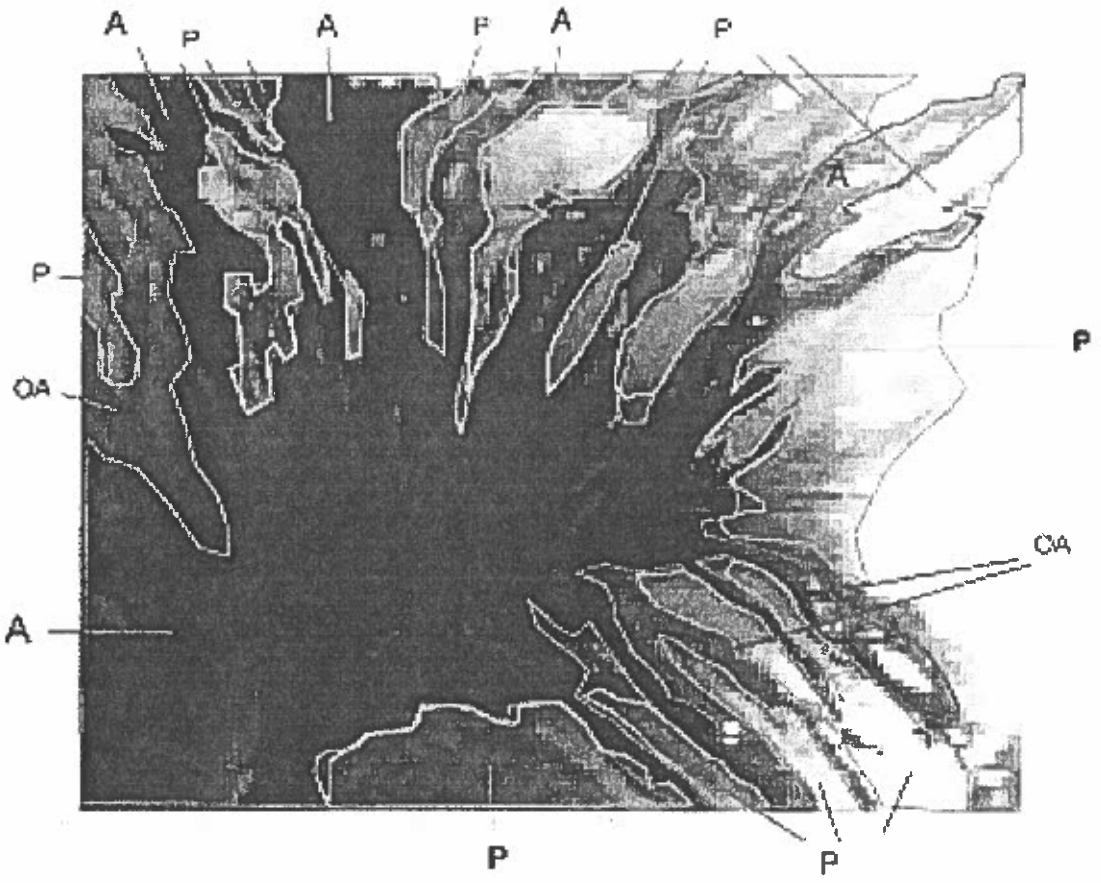

Figure A5- MODIS image at 250 m spatial resolution; near-IR (0.84-0.88 μm); flows becoming detectable, but not as clear as Figure A4.

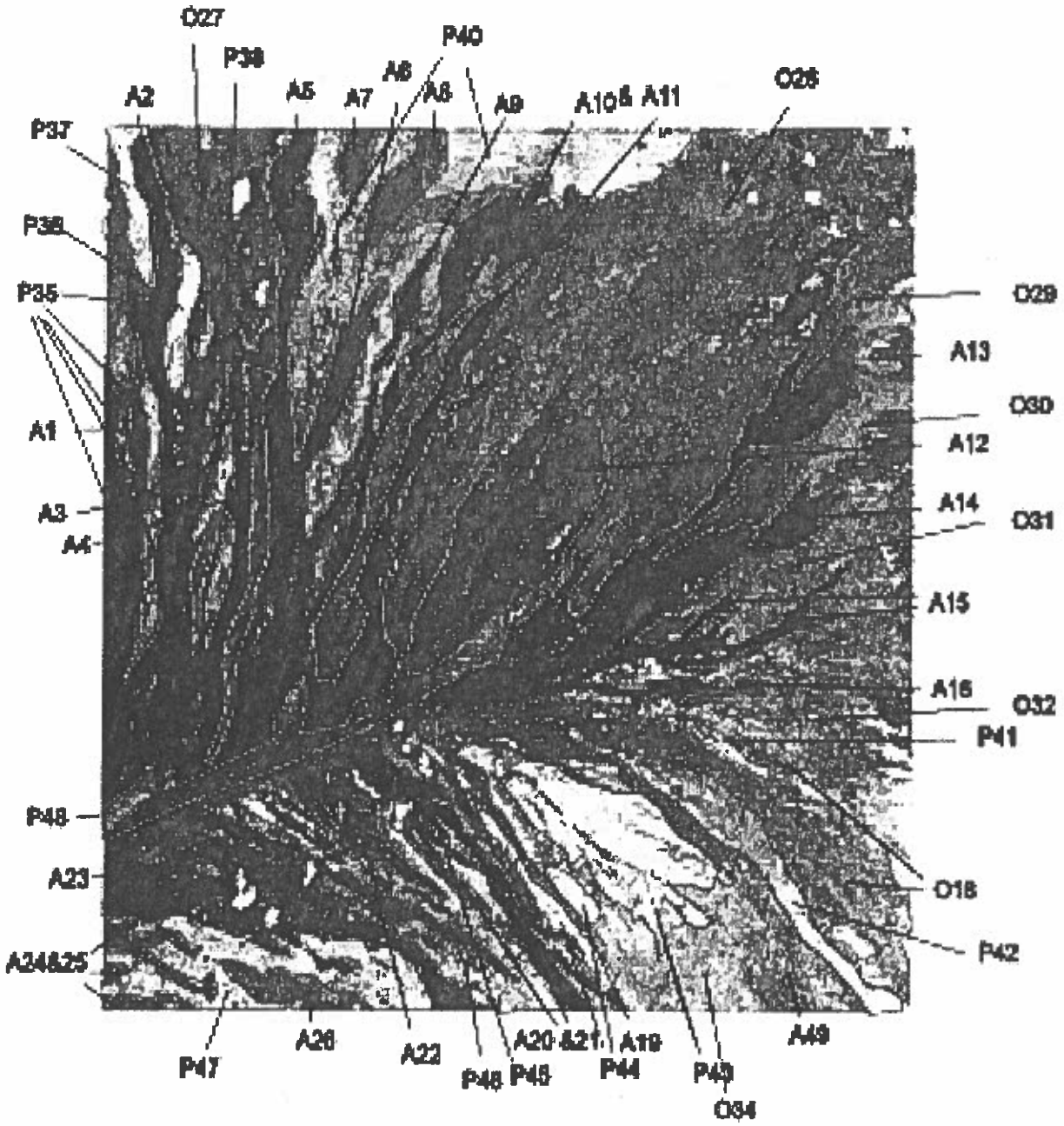

Figure A6- MSS image at 60 m spatial resolution; green visible (0.52-0.6 μm). Individual flows are now recognizable, and each flow is identified by a number

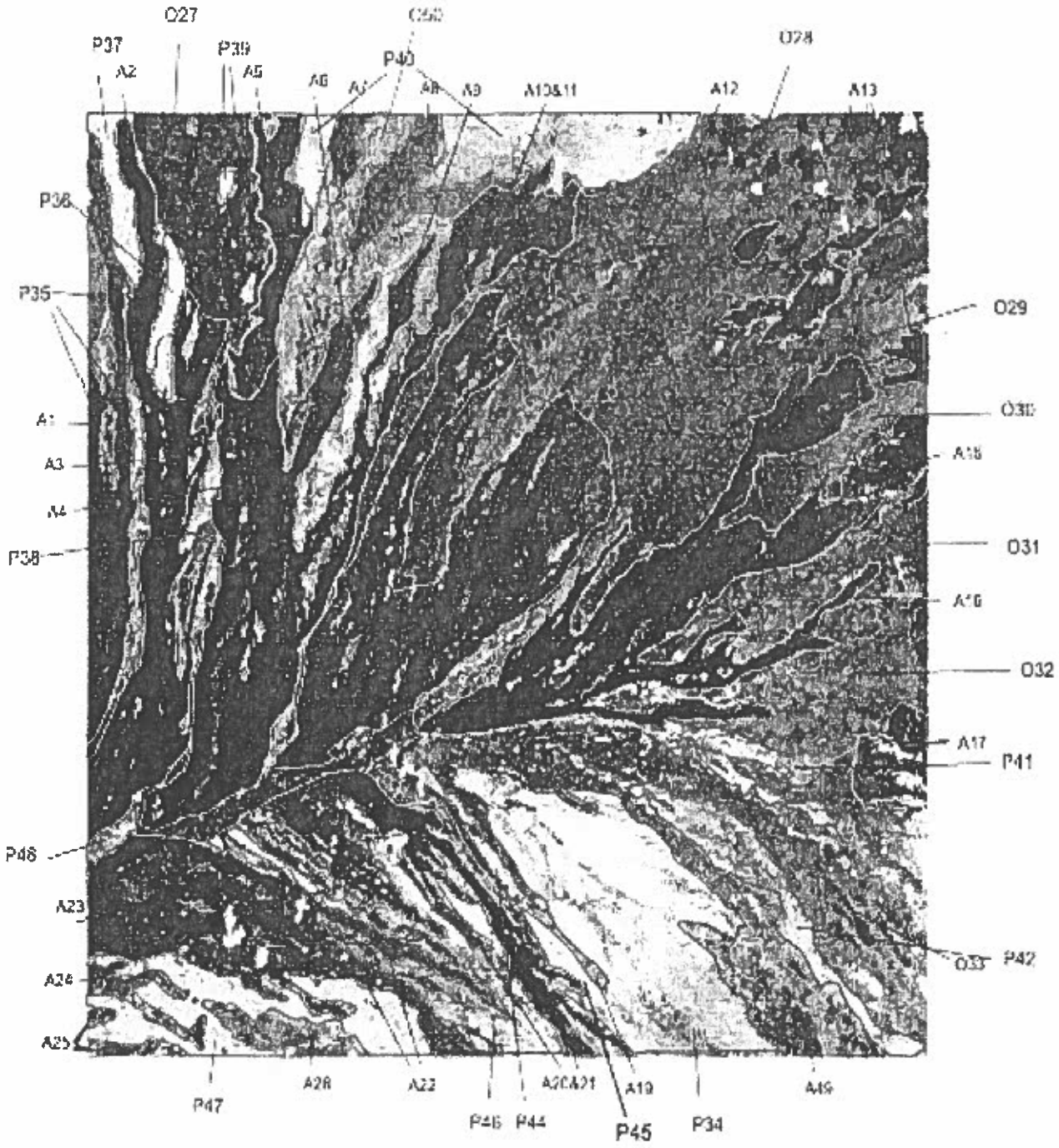

Figure A7- MSS image at 60 m spatial resolution; red visible (0.63-0.69 µm). Individual flows are recognizable and assigned the same numbers as in Figure A6

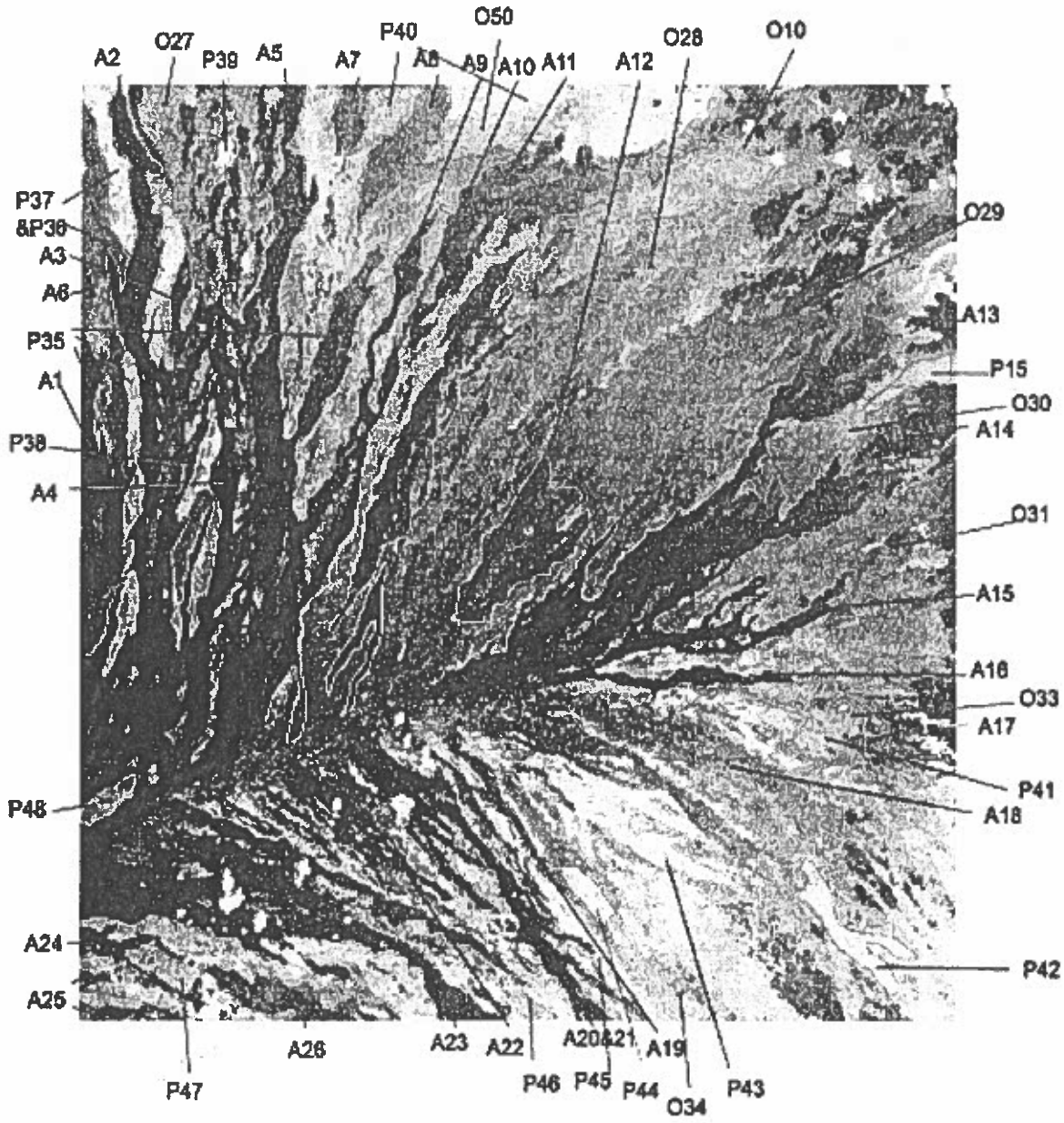

Figure A8- Landsat TM image at 30 m spatial resolution; blue visible (0.45-0.52 μm). Flows becoming more distinct, and more margins are noticeable.

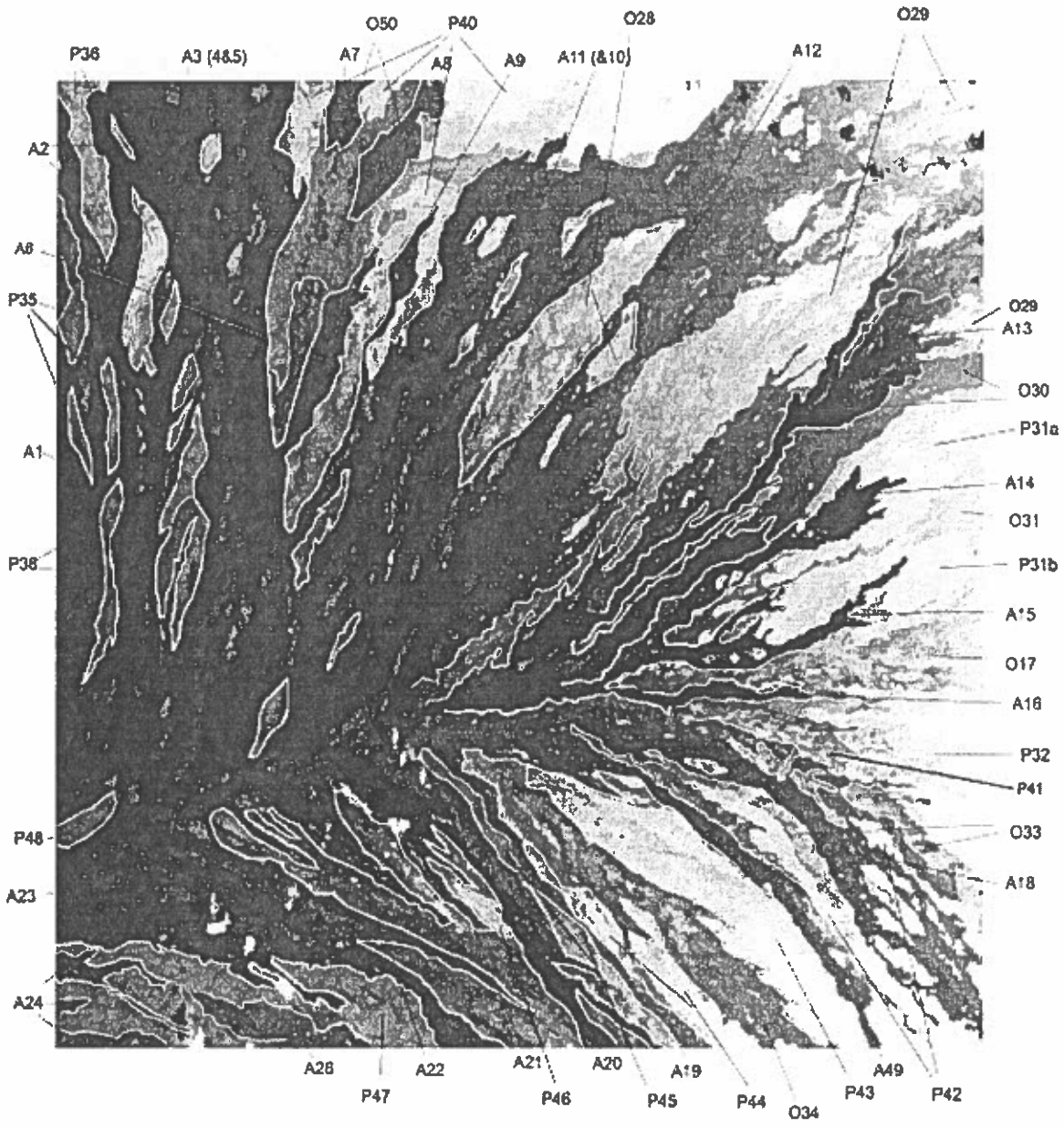

Figure A9- Landsat TM image at 30 m spatial resolution; near-IR (0.75-0.90 μm). Approximately the same number of flows are visible in this image as in Figure A8.

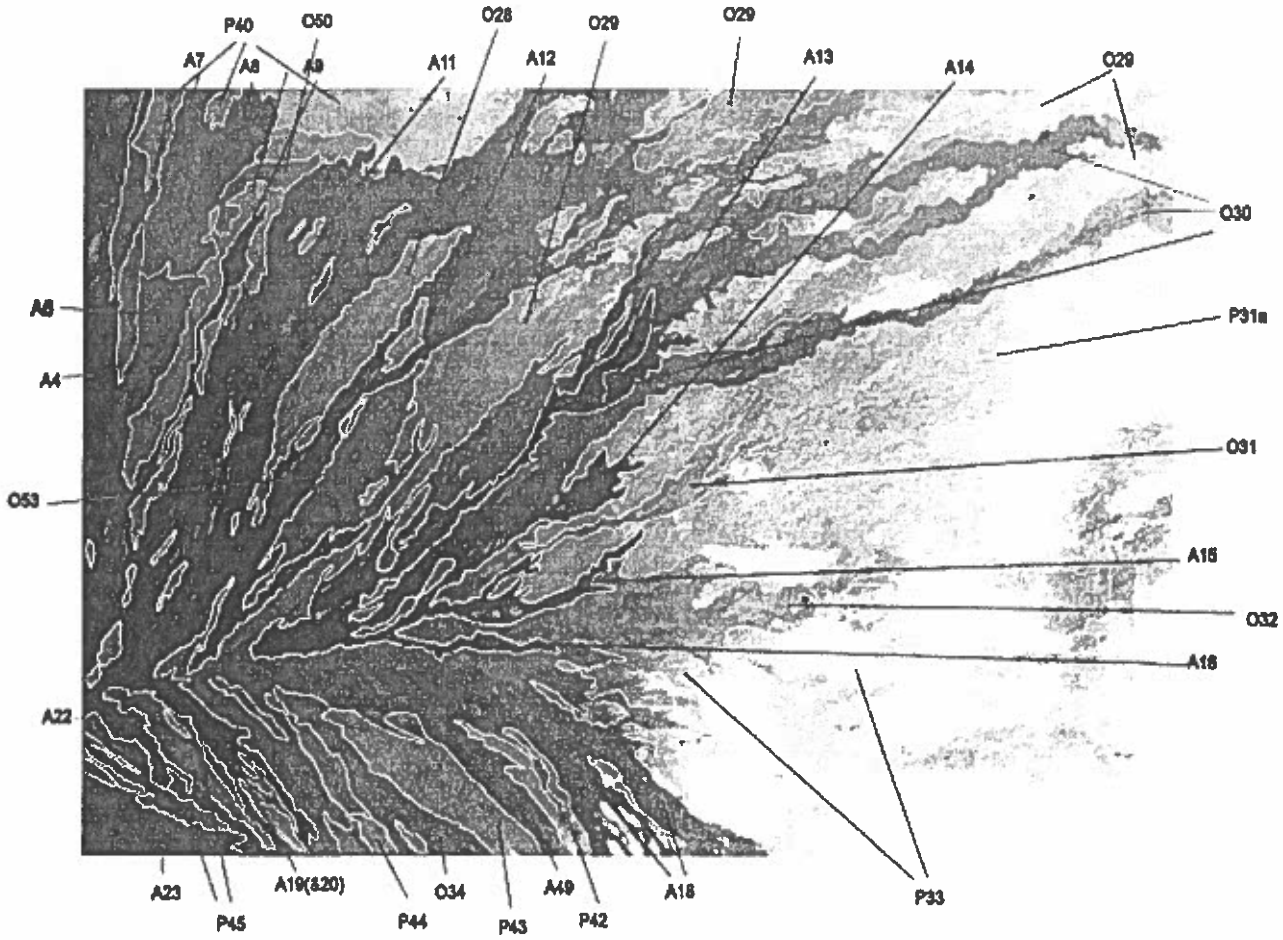

Figure A10- SPOT image at 20 m spatial resolution; near-IR (0.75-0.90 μm). Image shows fewer flows because total coverage is lower than the Landsat TM images

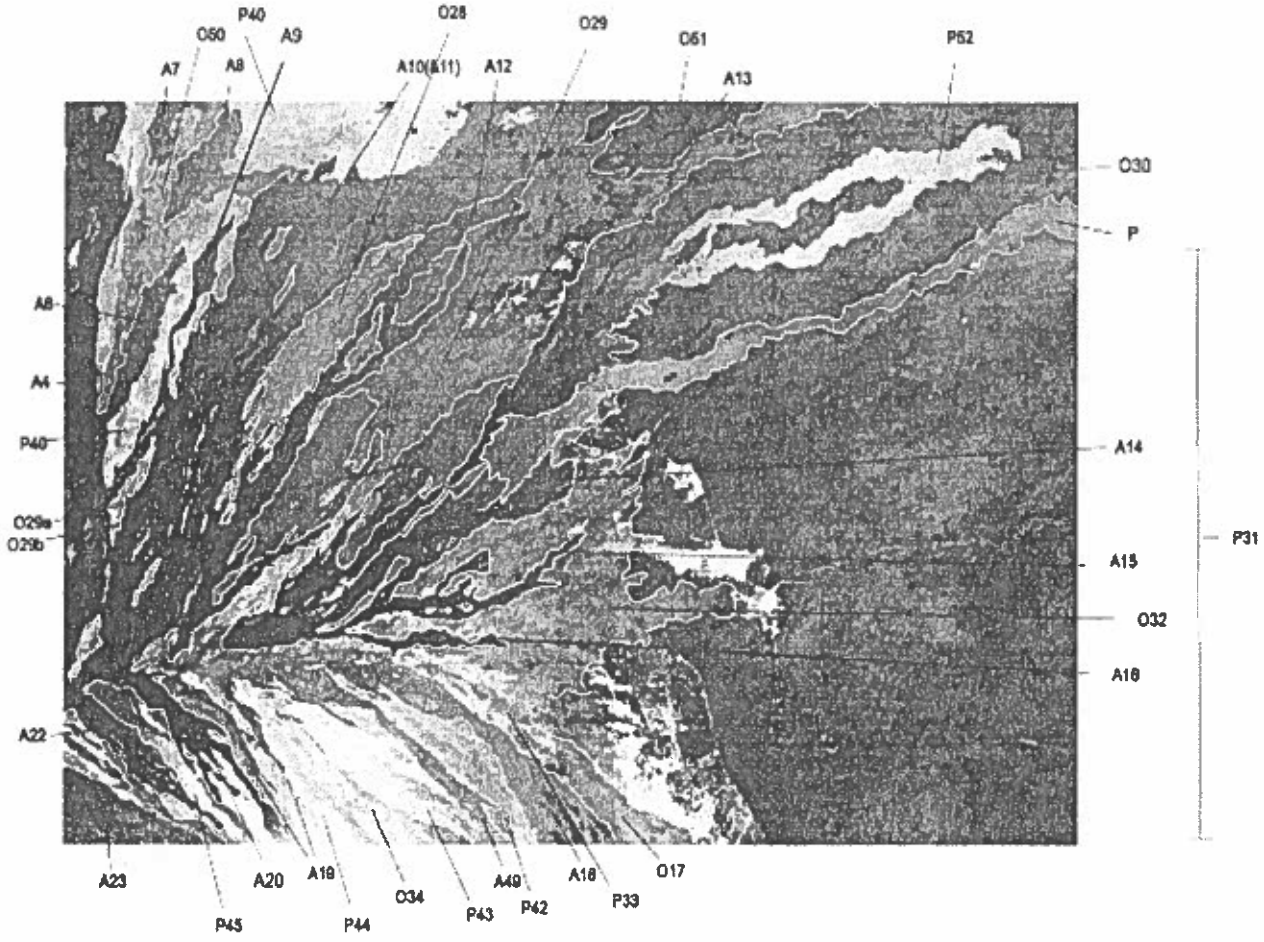

Figure A11- SPOT image at 20 m spatial resolution; red visible (0.63-0.69 μm). Slight shifts in albedo from Figure A10 cause some flow assignment changes.

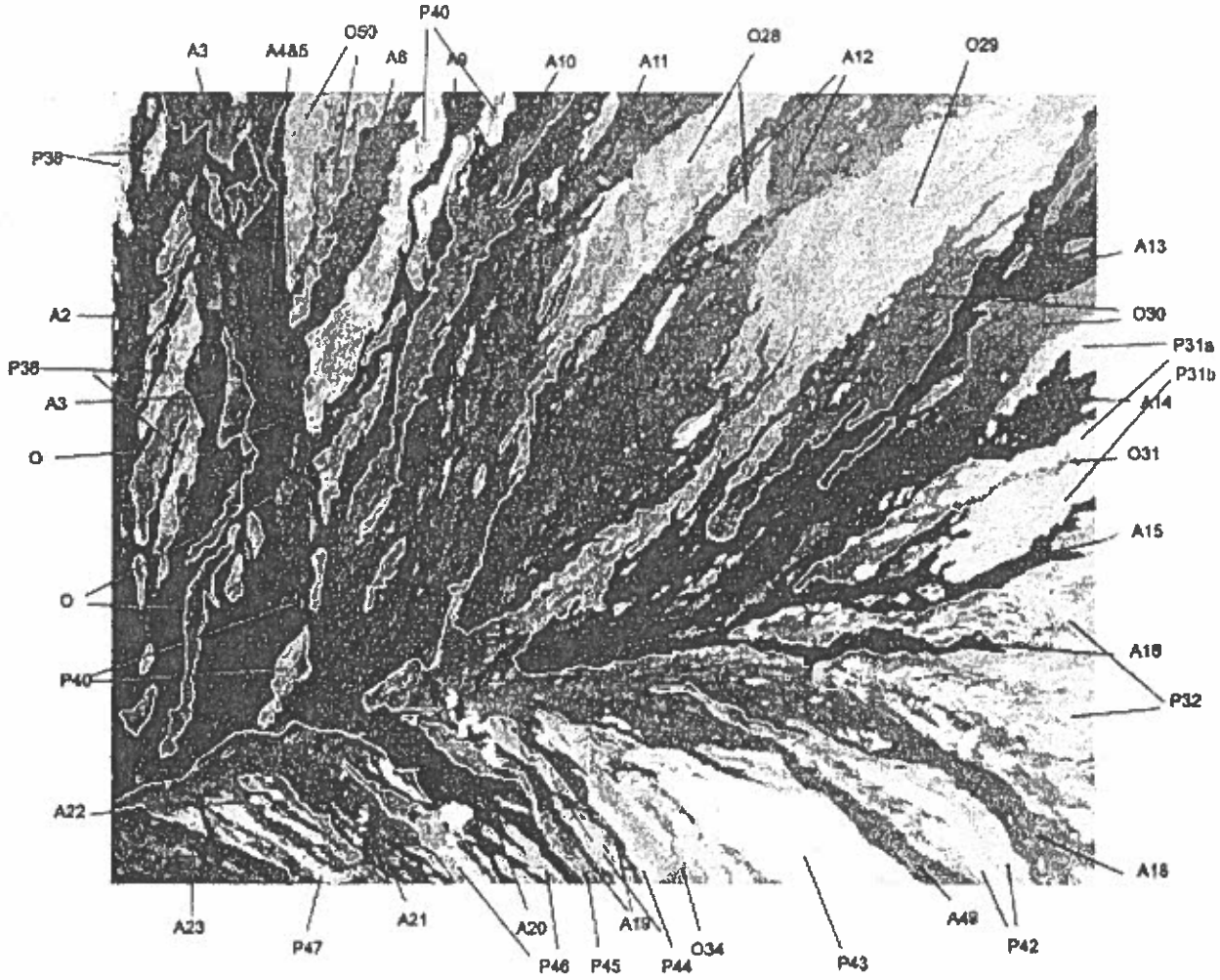

Figure A12- Landsat TM image at 15 m spatial resolution; all visible (0.52-0.90 µm). More flows detected in this image than in Figure A11 because area of image is larger.

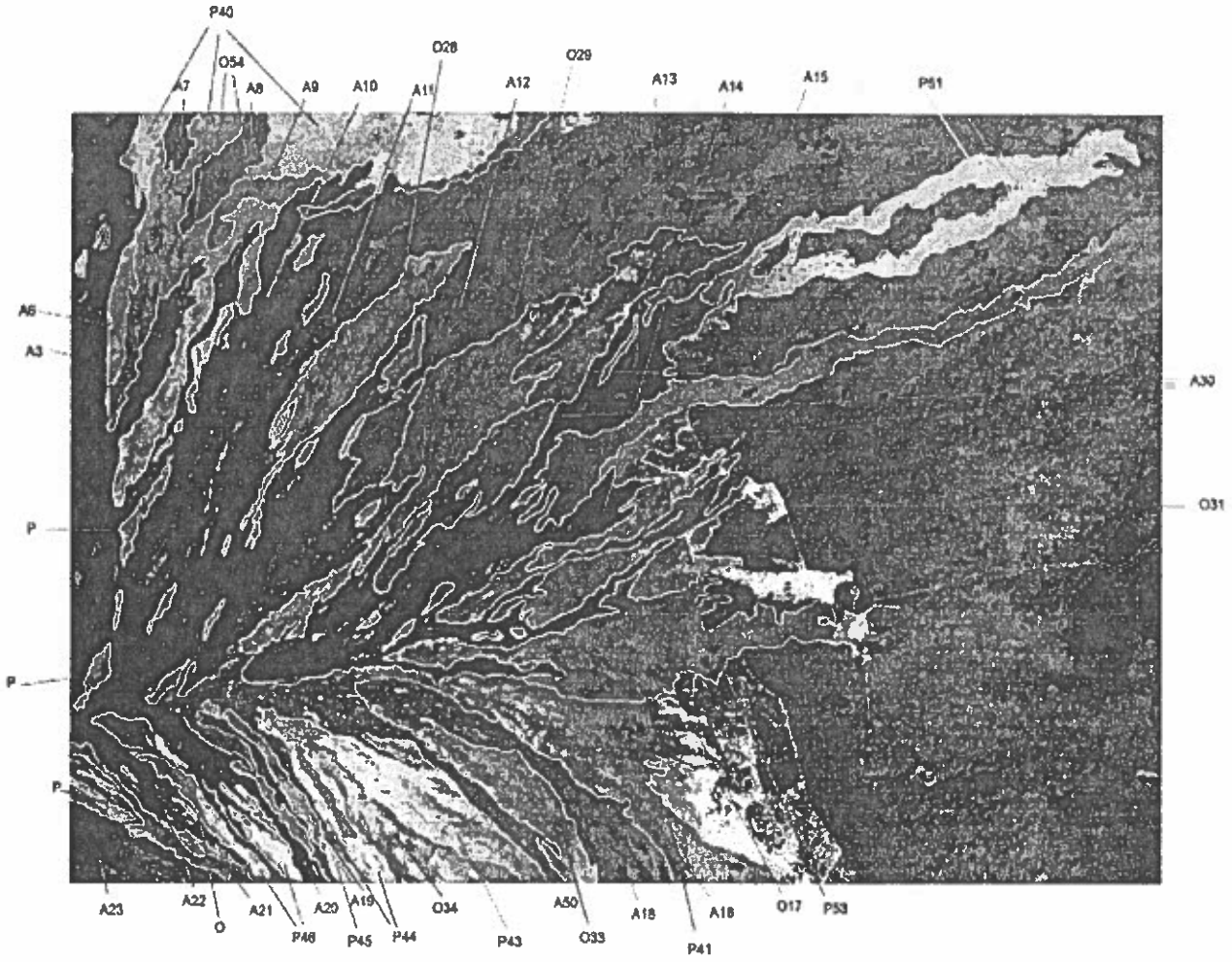

Figure A13- SPOT image at 10 m spatial resolution; all visible (0.52-0.90 μm). Fewer flows detected than in Figure A12 because total area coverage is not as large.

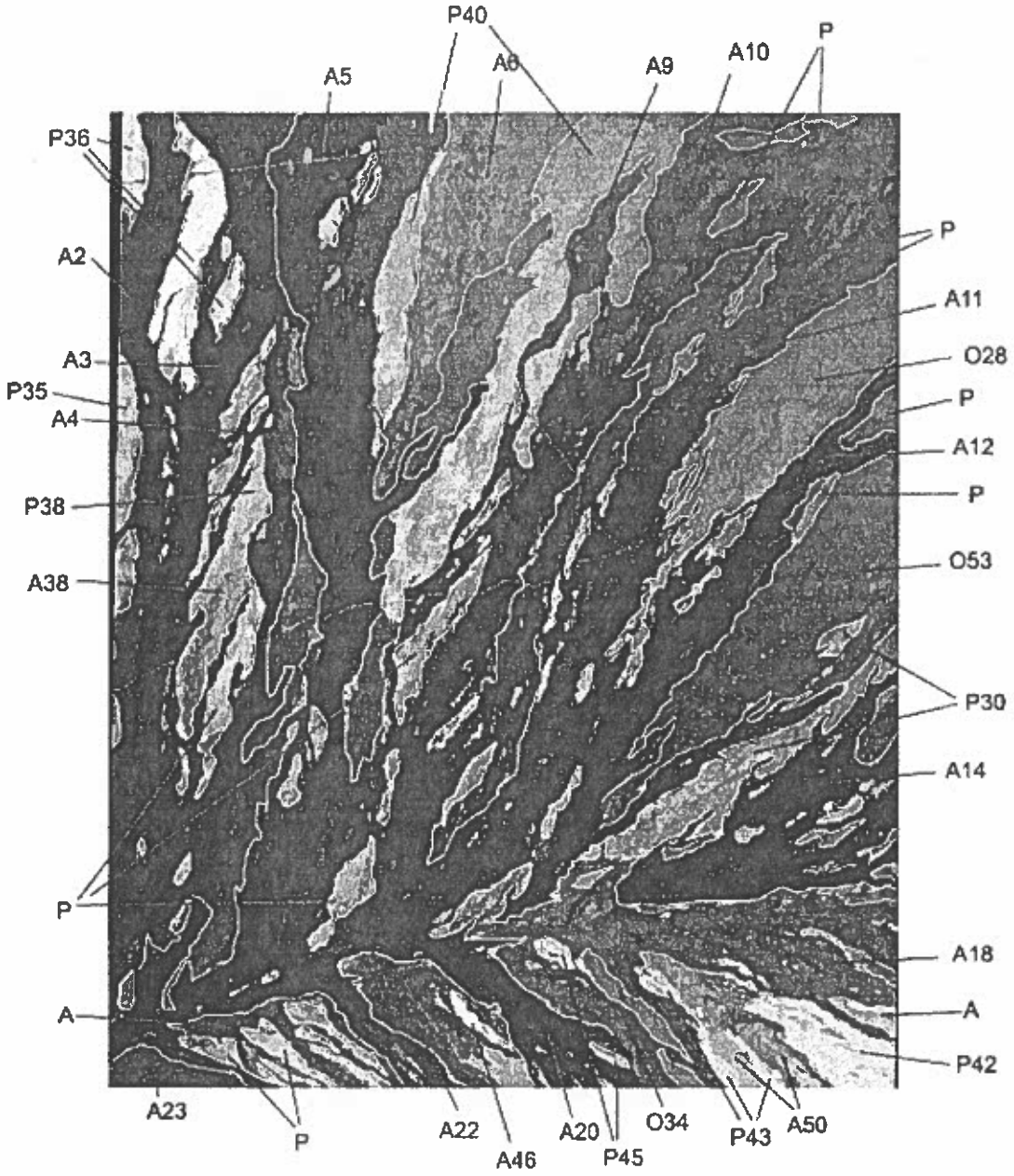

Figure A14- IKONOS image at 4 m spatial resolution; red visible (0.63-0.69 μm). Flows characteristics are much clearer than all other images.

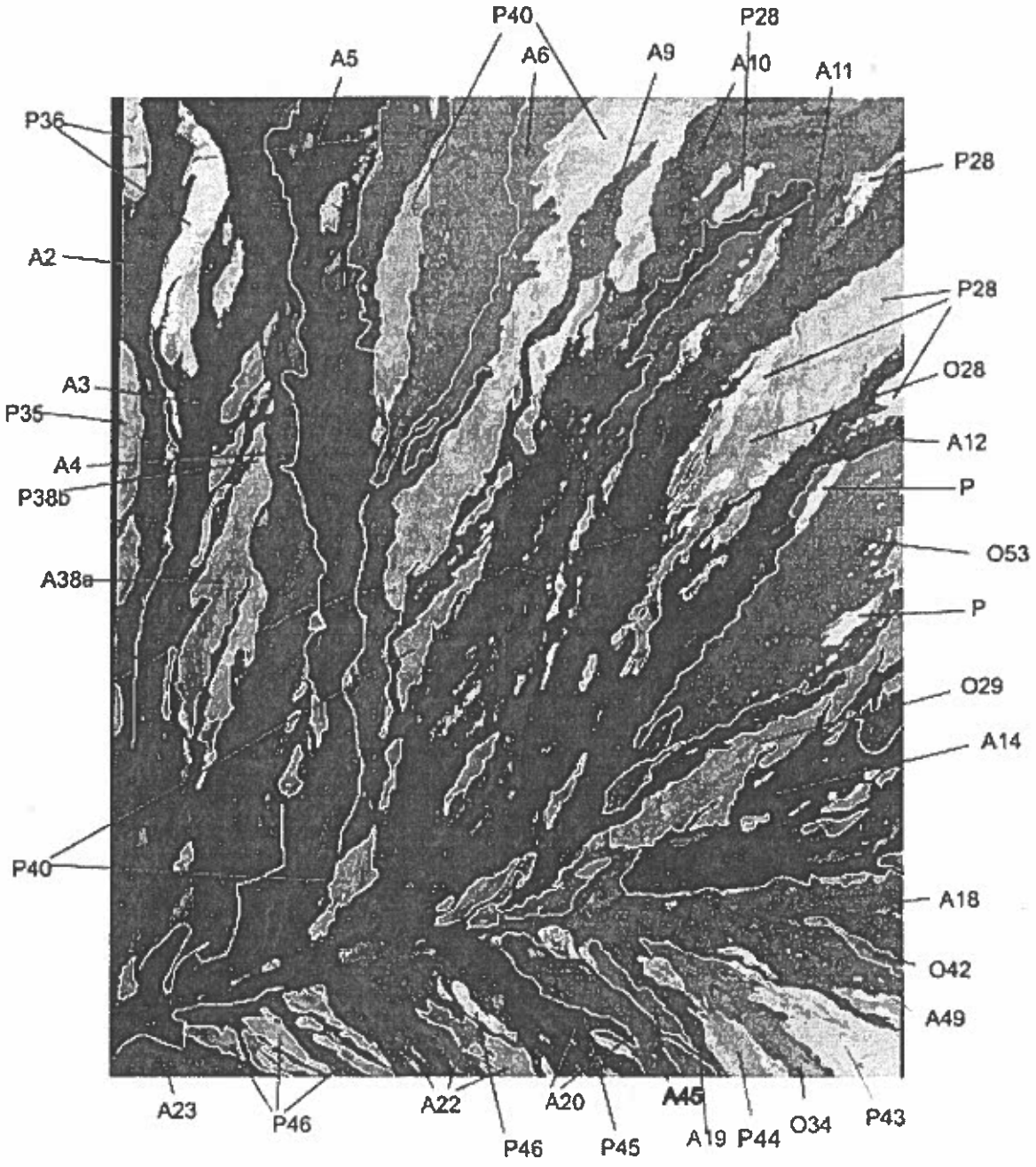

Figure A15- IKONOS image at 4 m spatial resolution; near-IR (0.75-0.90 μm). Flow characteristics are much clearer than all images of coarser spatial resolutions.

References

Bruno, B.C., Taylor, G.J., Rowland, S.K., and Baloga, S.M., (1994), "Quantifying the effect of rheology on lava-flow margins using fractal geometry", Bulletin of Volcanology, vol. 56, pp. 193-206.

Cashman, K.V., Thornber, C., and Kauahikaua, J.P., (1999), "Cooling and crystallization of lava in open channels, and the transition of Pāhoehoe Lava to 'A'ā", Bulletin of Volcanology, vol. 61, pp. 306-323.

Chernicoff, Stanley, (1999), Geology: An Introduction to Physical Geology, Houghton Mifflin Company, Boston, MA, Ch. 4 "Volcanoes and Volcanism", pp. 92-127.

Jensen, John R., (2002), Remote Sensing of the Environment: An Earth Resource Perspective, Prentice-Hall Inc., NJ.

Macdonald, Gordon, A., (1953), "Pahoehoe, Aa, and Block Lava", American Journal of Science, vol. 251, pp. 169-191.

Mouginis-Mark, P., and Wilson, L., and Zuber, Maria, T., (1992), "The Physical Volcanology of Mars" in Mars, edited by H.H. Kiefer, B.M. Jakosky, C.W. Snyder, and M.S. Matthews, Univ. of Arizona Press, Tucson, pp. 424-451.

Peterson, D.W., and Swanson, D.A., (1974), "Observed Formation of Lava Tubes (During 1970-71 at Kilauea Volcano, Hawaii", Studies in Speleology, vol. 2, pp. 209-221.

Peterson, D.W., and Tilling, R.I., (1979), "Transition of Basaltic Lava from Pahoehoe to Aa, Kilauea Volcano, Hawaii: Field Observations and Key Factors", Journal of Volcanology and Geothermal Research, vol. 7, pp. 271-293.

Rowland, S.K., and Walker, G.P.L., (1990), "Pahoehoe and aa in Hawaii: volumetric flow rate controls the lava structure", Bulletin of Volcanology, vol. 52, pp. 615-628.

Wilson, L., and Head III, J.W., (1983), "A comparison of volcanic eruption processes on Earth, Moon, Mars, Io and Venus. Nature, 302.21, 663-669.

Wilson, L., and Head III, J.W., (1994), "Mars: Review and analysis of volcanic eruption theory and relationships to observed landforms. Rev. Geophys., 32,3,221-263.